Detection Systems for Range Monitoring in Proton Therapy: Needs and Challenges

Pausch, G.; Berthold, J.; Enghardt, W.; Römer, K.; Straessner, A.; Wagner, A.; Werner, T.; Kögler, T.;

Originally published:

September 2018

Nuclear Instruments and Methods in Physics Research A 954(2020), 161227

DOI: https://doi.org/10.1016/j.nima.2018.09.062

Perma-Link to Publication Repository of HZDR:

https://www.hzdr.de/publications/Publ-27073

Detection systems for range monitoring in proton therapy: Needs and Challenges

Guntram Pausch,[a,b,*] Jonathan Berthold,[c] Wolfgang Enghardt,[a,b] Katja Römer,[d] Arno Straessner,[c] Andreas Wagner,[d] Theresa Werner,[a,b] and Toni Kögler[a,b]

[a]*OncoRay – National Center for Radiation Research in Oncology, Faculty of Medicine and University Hospital Carl Gustav Carus, Technische Universität Dresden, Helmholtz-Zentrum Dresden - Rossendorf, 01307 Dresden, Germany*

[b]*Helmholtz-Zentrum Dresden-Rossendorf, Institute of Radiooncology – OncoRay, 01307 Dresden, Germany*

[c]*Technische Universität Dresden, Institute for Nuclear and Particle Physics, 01069 Dresden, Germany*

[d]*Helmholtz-Zentrum Dresden-Rossendorf, Institute of Radiation Physics, 01328 Dresden, Germany*

Abstract

In-vivo range verification has been a hot topic in particle therapy for about two decades. In spite of vast efforts made by research groups all over the world, clinical devices and procedures for routinely monitoring the range of therapeutic particle beams in the patient's body and to ensure their correspondence with the treatment plan are not yet available. The paper reviews recent approaches with focus on prompt-gamma based methods of proton range verification and points to challenges that have not been discussed with the necessary depth and rigor in many (even recent) publications: First, the macro time structure of treatment beams in common proton therapy facilities requires detection systems with extreme load tolerance, throughput capability, and stability against load leaps. Second, the time period available for verifying the range of a single pencil beam spot is of the order of milliseconds, which limits the number of prompt gamma events that can be detected and processed. In view of these constraints it might be favorable to waive tight event selection by collimation or coincidence conditions as applied in most prompt-gamma based range verification techniques considered so far, and to move on to straight detection with uncollimated detectors combined with a multi-feature analysis deploying all pieces of information comprised in a registered event. Energy deposition, timing, and energy sharing between the involved detector segments in case of Compton-scattering or pair production are parameters bearing information on the beam track that could be extracted in a comprehensive analysis. This would maximize the number of valid events on the expense of 'information sharpness', but could eventually increase the total yield of information exploitable for range verification. Some aspects of such a strategy have already been realized with the Prompt Gamma-Ray Timing (PGT) and the Prompt Gamma Peak Integration (PGPI) techniques proposed recently. Data analysis schemes for a more generalized approach have not yet been developed, but the hardware to be used can already be sketched: Prompt gamma rays should be detected with scintillation detector modules consisting of single pixels with individual light readouts and independent electronic channels, similar to those developed for PET-MR. Prompt gamma-ray detection in this context is, however, much more demanding with respect to dynamic range,

* Corresponding author. Tel.: +49-351-458-7414; fax: +49-351-458-7263; e-mail: guntram.pausch@oncoray.de

energy resolution, load acceptance, and stability. The corresponding requirements represent a challenge for the detector physics community.

Keywords: Proton therapy; particle therapy; range verification; prompt gamma ray; Compton camera; gamma camera;

1. Introduction

Particle therapy (PT) has become a widely accepted and promising option for tumor treatments, complementing the conventional radiotherapy performed with megavolt X-rays and electrons. Meanwhile, more than 70 facilities all over the world can provide beams of protons, carbon or other ions for clinical treatments [1]. The well-defined range of ions in tissue with the final dose maximum (Bragg peak) followed by a sharp distal dose fall-off allows focusing the dose in the tumor while minimizing the damage of surrounding normal tissue. The accuracy of predicting (i.e., planning) the range in tissue is, however, affected by uncertainties in converting CT images in stopping power maps, by anatomical changes in the patient's body during the treatment, and by other factors that are hard to assess in clinical routine [2]. These uncertainties lead to rather large safety margins in the treatment planning and constrain potential benefits of particle over conventional therapies [3]. The reduction of range uncertainties would improve the precision and reduce the normal-tissue toxicity of particle therapy. In this context, considerable efforts have been made to develop clinically applicable instruments for verifying the particle range in situ, just during dose delivery, ideally with a precision of one or two millimeters [4].

In spite of these efforts, commercial instrumentation for range monitoring is not yet available. This seems astonishing in view of the many papers on this topic that have been published since the 1990ies. However, clinical environment and clinical workflow in a particle therapy facility put severe constraints on an instrument design:

(i) A range verification system (RVS) must neither interfere with the treatment beam nor with the patient who is usually positioned on a robotic couch. In case of a treatment gantry, the RVS should be gantry mountable. This limits the acceptable size and weight.

(ii) The range verification procedure must not extend the time a patient has to stay in the treatment room. This is a question of resource economy. Clinics have to take care for a high

patient throughput in order to justify and to refund considerable investment and operational costs of a PT facility.

(iii) Range verification systems must cope with the time structure and intensities of treatment beams as given by the therapy facility and treatment planning rules. Physicians (and, accordingly, manufacturers of PT facilities) try to keep irradiation times as short as possible. This reduces the patient's strain as well as the risk of positioning errors caused by unwanted motions of a patient. It is useless to hope that treatments could be lengthened to relax demanding conditions for an RVS.

Unfortunately the latter aspect has been ignored in many (also recent) papers dealing with range verification techniques. Therefore we will exemplify so-called 'treatment conditions' in a common, commercial proton therapy facility, and discuss constraints resulting for the construction of RVS. Finally we justify a generalized concept to overcome load and statistics issues in range verification based on prompt gamma rays, and derive key parameters for corresponding detection systems.

2. State of the art in range monitoring

As a matter of principle, therapeutic particle beams stop in the patient's body. Any non-invasive technique of range monitoring must therefore rely on secondary signatures, namely signals that are generated by the beam, bear information on its location or range, and escape the body.

Particle-therapy PET, developed in the 1990ies, was the first method of in-vivo range verification that has ever been successfully applied in patient treatments with particle beams [5]. PT-PET measures the β^+ activity distribution induced by the ion beam crossing tissue with a common (commercial) or a dedicated (in-beam) PET scanner. The main disadvantage of PT-PET is the signal delay of seconds to minutes in correspondence with the respective decay times of the β^+ emitters. It causes a conflict between optimum measurement conditions and the constraints (i) and (ii) named in section 1: The PET scan should best start during the treatment and then continue at least some minutes after. This maximizes collectible statistics and minimizes washout effects [6], thus leading to an optimum image quality. In-beam PET measurements, however, could only be performed with a scanner that does not interfere with the beam (a question of the mechanical design) and is not blinded by the prompt gamma-ray flash during dose delivery (a question of detector technology and signal processing). Even if

dedicated instrumentation was available, the prolonged measurement after beam delivery compromised the clinical workflow and reduced the patient throughput. That is why applications of in-beam PET are restricted to clinical studies performed with non-commercial scanners, usually built by research teams [5] [7]. The economically more efficient solution fitting with the mentioned constraints, namely measurements with a commercial PET scanner after moving the patient to another room, suffers from much lower statistics and the consecutive disturbance of the primary correlation between β^+ activity distribution and spatial dose deposition in the patient due to biological washout by metabolism, blood and lymph circulation [6].

That is why many research groups have focused their efforts on a promising alternative, namely range verification based on prompt gamma rays (PG). This hard radiation is produced in nuclear reactions triggered by beam particles hitting atomic nuclei of the penetrated tissue. It is emitted along the beam track and well correlated with the dose deposition [8]. Prompt gamma-ray imaging (PGI) can thus be used to reconstruct the beam track in tissue. Imaging systems with passive collimation by a pin-hole [9], a linear slit [10], or multiple slits [11], have been investigated. So far the Knife-Edge Slit Camera [12] developed by IBA[1], a company providing proton therapy facilities and related equipment, is the only system that has ever been used for range monitoring in clinical treatments [13] [14]. This camera is capable of detecting local range shifts down to 1-2 mm [15]. However, the massive and heavy collimator may interfere with the patient's position and makes integration in a treatment facility an expensive challenge. So it seems obvious to use active collimation instead. Several groups have tackled the challenge of Compton imaging in the prompt-gamma energy domain [16] [17] [18] [19] [20] [21] [22] [23]. Technical complexity, electronic expense, the huge detector load to be handled during dose delivery, the low fraction of 'valid' events and the remaining background after passing all coincidence and event selection criteria are intrinsic hurdles that cast doubts on the applicability of Compton imaging under therapy conditions [20] [21] [22], in spite of punctually encouraging results [23].

Some recent approaches are based on straight detection of prompt gamma rays with common, unsegmented scintillation detectors:

[1] IBA Ion Beam Applications S.A., https://iba-worldwide.com/

- Prompt gamma-ray spectroscopy (PGS) measures intensity ratios of characteristic prompt-gamma lines with detectors of adequate energy resolution [24]. The field of view of these detectors is restricted to a distinct section of the beam track by using a massive slit collimator. The reaction channels feeding the gamma lines are distinguished by specific energy dependencies of the corresponding cross sections. Line intensity ratios therefore measure the actual beam energy at the point of observation, or the residual range of beam particles at the depth the collimated detector is looking at. An elaborated setup for clinical use, consisting of a heavy collimator, multiple commercial $LaBr_3$:Ce detectors, and a high-throughput data acquisition system, is close to first testing in patient treatments [25].

- Prompt gamma-ray timing (PGT) analyzes the time distribution of prompt gamma rays generated by a micro-bunched particle beam [26]. PGT spectra are measured with uncollimated detectors relative to a bunch timing signal, actually the accelerator radiofrequency (RF) tapped from the therapy facility [27] [28]. The setup resembles a common time-of-flight (TOF) measurement. The width of the timing peak comprising prompt events reflects the width of the time window for prompt gamma-ray emissions, which equals the finite stopping time of the beam particles in tissue. The latter is defined by the particle kinematics and is sensitive to their range. Tests with simple phantoms under close-to-clinical conditions have proven the principle and yielded encouraging results [29].

- Prompt gamma peak integration (PGPI) determines the Bragg-peak position from prompt-gamma count rate ratios measured with multiple detectors arranged around the target [30], i.e., the patient's body. The individual count rates depend on the detectors' distance from beam track and Bragg peak but are disturbed by interactions of the emitted radiation with the body. Supposed the scattering and absorption effects could be corrected for, the count rate ratios provided means for a range measurement. This technique has been demonstrated in a simplified test case; its applicability in clinical scenarios has not yet been evaluated.

These three methods make use of common detector technologies and straight data acquisition without event preselection by trigger or multiplicity logics. This promises simplicity, robustness, and reduced expense.

A thorough and detailed review of PG-based range verification techniques is given in [31]. It is worth mentioning that each of the PG-based range monitoring techniques discussed so far essentially analyses just one distinct feature of the detected events: the incidence direction (correlated with the emission vertices) in case of PGI, the gamma-ray energy in case of PGS, the detection time in case of PGT, and the detection rate in case of PGPI. Complementary features are used for event filtering but not for extracting range information: Energy cuts, for instance, select the high-energy PG events to be used for PGT or PGI; time cuts are used to suppress uncorrelated background in case of PGI and PGS; passive collimators restrict the incidence angle of the gamma rays analyzed for PGS.

There are some other techniques of range verification that have been proposed and explored. Pencil beam proton radiography [32] can be used for checking the correctness of stopping power maps derived from the planning CTs at reasonable expense. It is, however, in conflict with constraint (ii) mentioned above since it requires patient scans with low-intensity beams in the treatment room. Beam track imaging by means of secondary-electron bremsstrahlung has been demonstrated with carbon [33] and proton beams [34], but the results can hardly be translated to treatment conditions. Acoustic methods [35] [36] could be of advantage in case of highest beam intensities. Such techniques, however, have only been explored in oversimplified scenarios and are by far not mature for clinical testing.

This paper focuses on techniques based on prompt gamma-ray measurements, since they are most promising and closest to clinical applications. The discussion is also restricted to range verification in proton therapy facilities. Those are cheaper and much more common than facilities providing beams of ^{4}He, ^{12}C, or other ions as well, and their number is growing steadily.

3. The load and statistics problem

PG-based range assessment in proton therapy is faced with a serious problem posed by intensity and time structure of typical treatment beams. This becomes evident if one considers key parameters of an exemplary clinical treatment site.

Let us look, for instance, at the IBA Proteus®PLUS facility of the University Proton Therapy Dresden (UPTD). It is equipped with a universal nozzle capable of providing double-scattering (DS) as well as pencil-beam scanning (PBS) treatments. Meanwhile most treatments are delivered in PBS mode. This is the most advanced, most economic and gentle technique of dose delivery in recent

clinical facilities. The tumor is scanned in three dimensions with a beam focused to about the diameter of a pencil (0.5 to 1.5 cm FWHM). Lateral beam deflection by dipole magnets provides two scanning dimensions, the third one is due to a stepwise variation of the beam energy and consequently of the penetration depth (range). A PBS treatment plan is organized in so-called energy layers, each comprising a finite number of beam spots ('single pencil beams' or PBS spots) of the same beam energy but different lateral positions as defined by settings of the scanning magnets. These spots are typically delivered within 2-10 ms and separated by beam breaks of about 1 ms duration for updating the magnet settings. The energy layers, on the other hand, are separated by two-seconds breaks needed for beam energy switching. Note that the IBA C230 cyclotron is, as most proton therapy accelerators, a fixed-energy machine. The beam energy is actually set by a degrader of varying thickness, followed by an energy selection system comprising an analyzing dipole magnet and slit collimators.

The macro time structure of PBS treatments can be visualized by monitoring the prompt gamma-ray production rate. Figure 1 presents an exemplary count rate histogram measured with a PGT detection unit [37] during delivery of a representative PBS treatment field to an anthropomorphic head phantom. The corresponding measurement was performed in parallel to the sensitivity evaluation of a knife-edge slit camera [15]. The histogram relates to the intensity-modulated proton therapy (IMPT) treatment plan described in [15]. It comprises one of two irradiation fields of a single fraction, representing a dose delivery of about 1 Gy (photon-equivalent dose) to the target volume. The left panel illustrates the coarse structure. Energy layers can be clearly distinguished. The built-up β^+ activity causes a variable pedestal in between the layers. A closer look in a single layer (right panel) reveals the varying beam current (in terms of the count rate), spot duration, and spot strength (number of protons in a spot reflected in the number of prompt gamma-ray detections).

Figure 1

In a PBS treatment, *spatially* resolved range verification means assessing the *individual* ranges of distinct PBS spots. Range verification systems must therefore in general extract the necessary

information from statistics that can be collected during delivery of a single spot, which means in a measuring period of 10 ms or less. Furthermore they have to cope with a detector load as defined by the maximum rate of proton delivery in the strongest beam spots.

Figure 2 shows the distribution of spot strengths (proton numbers) for the same treatment field. In accordance with a similar analysis published earlier [10], the spots comprise up to $1\text{-}2\times10^8$ protons. 10^8 can be considered as representative number of protons for strong (mostly distal) PBS spots; there are, in general, are only few spots exceeding this limit. If delivered in 10 ms, this corresponds to a rate of 10^{10} protons per second or a pencil beam current of about 2 nA, which is in good agreement with the regular current at nozzle exit stated for the given facility. Assuming a prompt gamma-ray production yield 0.1-0.3 per proton [10] [38], this translates to $1\text{-}3\times10^7$ prompt gamma rays per spot emitted in 4π, and to a production rate of $1\text{-}3\times10^9$ s^{-1} during spot delivery. In other words: There are plenty of prompt gamma rays per spot, but the time available for a range measurement is extremely short. The statistics of 'usable' PG events per spot is then not essentially given by the detector efficiency, but rather by the acceptable detector load, by the achievable system throughput, and finally by the fraction of events passing the respective event filter criteria.

Figure 2

Table 1 compiles some key numbers. The next sections exemplarily analyze consequences and limitations resulting for range verification systems on the basis of two representative RVS concepts described in previous papers, namely a Compton imaging setup and a system based on straight PG detection.

Table 1

3.1. Random and combinatorial background in systems based on coincidence measurements

Prompt gamma-ray imaging with Compton cameras has been explored by many research groups around the world, as summarized in [31]. Most of the published papers, however, are simulation studies. Only few systems have ever been tested with radioactive sources, and so far – to the authors' best knowledge – only one Compton camera system could demonstrate reasonable imaging of a proton pencil beam in a clinical facility, though not yet with clinical beam currents [23]. We take this system as a reference to discuss limitations for RVS based on coincidence measurements.

The imaging setup described in [23] is based on four POLARIS-J^{TM} detection stages by H3D[2] comprising large-volume, pixelated Cadmium Zinc Telluride (CZT) detectors of excellent energy resolution. The authors state a single gamma-ray detection rate of 54 kcps at 0.52 nA beam current [23]. This detector load should be basically due to prompt gamma rays. If we assume an average prompt gamma-ray production yield of 0.15 per proton, the 0.52 nA beam would generate about 5×10^8 prompt gamma rays per second. We can therefore estimate the absolute PG detection efficiency to about 0.01 % per detector stage or ε = 0.04 % for the complete 4-stage system. Considering the 'D2C' filter applied for suppressing events that are not suited for image reconstruction, this system provides about 1.5×10^{-6} usable events per incident proton [23]. This means not more than 150 valid (D2C filtered) events per PBS spot of 10^8 protons. This is a rather low number for detecting the end of a pencil beam track with millimeter precision since the gamma emissions are more or less randomly distributed along the beam track. The authors propose enlarging the setup by using 12 instead of only 4 detection stages.

However, another parameter given is the coincidence resolution time of τ = 1.5 μs [23]. Events with detection times differing by not more than τ are assumed to form a Compton-scatter event induced by an incoming prompt gamma ray. Random coincidences occur if at least one other of the many gamma rays hitting the system generates an interaction within the time interval τ following a first detection. The corresponding probability is, according to [39], given by

$$P_{rand} = 1 - P(0)$$

where

[2] H3D, Inc., https://h3dgamma.com/specialtyProducts.php

$$P(0) = e^{-r\tau} = e^{-\varepsilon R\tau}$$

means the probability to detect *no* other hit in the time interval τ following a first detection, r the true event rate, R the total gamma production rate, and ε the absolute gamma detection efficiency of the system.

As a matter of principle the fraction of registered Compton events that are not contaminated with an additional gamma-ray detection in the coincidence time window somewhere else cannot exceed $P(0)$. Therefore rate of true coincidences due to (undisturbed) Compton-scatter events cannot exceed the value

$$r_{true}^{max} = r \cdot P(0)$$

Figure 3 exhibits the random coincidence fraction P_{rand} and the maximum true coincidence rate r_{true}^{max} for different coincidence resolution times τ as a function of the absolute system detection efficiency ε, calculated for a total gamma production rate of $R = 2\times10^9\,s^{-1}$ in accordance with Table 1. It is evident that random coincidences would represent at least about two thirds of the coincidence rate measured under treatment conditions with the 4-stage Compton camera system of 0.04% detection efficiency. With the larger 12-stage system of 0.12 % efficiency, random coincidences would by far dominate the acquired event rate; the fraction of true coincidences could not exceed 2%. Moreover, the wide coincidence window of 1.5 µs generally restricts the applicable detection efficiency. Once the efficiency reaches 0.03 %, a further increase does not rise but even reduces the maximum detectible rate of true coincidences caused by Compton scattering of a single gamma ray.

Figure 3

A weaker but more general limit of systems based on coincidence measurements is due to the simultaneous detection of two or more prompt gamma rays generated in the same micro-bunch. Such coincidences cannot a priori be distinguished from Compton-scattering events. According to Table 1, a

single proton micro-bunch generates up to 30 prompt gamma rays. Given a system with detection efficiency ε, the probability $P_{M(N)}$ of detecting just M out of the N prompt gamma rays per bunch is

$$P_{M(N)} = \binom{N}{M} \cdot \varepsilon^{M} \cdot (1-\varepsilon)^{N-M}$$

Corresponding single-hit ($M = 1$), multi-hit ($M > 1$), and total event rates ($M > 0$) are given by

$$r_{M=1} = f \cdot P_{1(N)}$$

$$r_{M>1} = f \cdot \sum_{m=2}^{N} P_{m(N)} = f \cdot (1 - P_{0(N)} - P_{1(N)})$$

$$r_{M>0} = f \cdot \sum_{m=1}^{N} P_{m(N)} = f \cdot (1 - P_{0(N)})$$

where f means the repetition rate of proton micro-bunches.

Figure 4 shows these rates as a function of the system detection efficiency ε for N = 20 and a micro-bunch frequency f = 106 MHz in accordance with Table 1. Obviously the 'combinatorial' background sets an absolute limit for the applicable system detection efficiency: If the detection efficiency approaches 5 %, the increase of the total detection rate is predominantly due to the growing rate of multiple detections. The single-hit rate saturates at $\varepsilon \approx 5$ % and finally decreases. Note that this limit is independent of the coincidence resolving time, at least as long as the time resolution is not in the few-picoseconds range.

Figure 4

It is evident that random coincidences affect the applicability of Compton imaging systems in clinical treatments. One could argue that intelligent event filtering would reduce the random fraction. However, filters are usually distinguished by finite efficiency and lower the rate of usable events. It is also clear that filtering cannot reduce the system load caused by the background. As shown in the

example, random coincidences could even dominate the acquired event rate. In any case, corresponding estimates and investigations have to be part of related research and must be considered in the instrument designs as well as in publications.

3.2. Load and throughput constraints in systems based on straight detection

The importance of load and throughput constraints can be best illustrated by looking at a system based on straight prompt gamma-ray detection. The PGT experiments at OncoRay have been performed with detection units consisting of common ∅2”×2” and ∅2”×1” $CeBr_3$ scintillation detectors by Scionix[3], coupled to high-throughput digital energy and timing spectrometers U100 by Target[4] [37]. The count rate plots shown in Figure 1 were measured with a ∅2”×2” detector at 40 cm distance from the isocenter while delivering the representative clinical treatment field describe above. During strong PBS spots the registered count rate was around 600 kcps (Figure 1, right panel). The U100 is distinguished by a fixed dead time of 1 µs per event. The throughput of 600 kcps then translates to a detector load of 1.5 Mcps relating to energy depositions above the trigger threshold of 80-100 keV. Though an asymptotic throughput of 1 Mcps could be achieved, a further increase of the detector load distinctly raises the percentage of system dead time as well as the fraction of pulse pileups. In PGT experiments performed with clinical beam currents at OncoRay, detector-target distances have mostly been chosen in the 40-60 cm range to keep detector loads well below 3 Mcps, best in the 1 Mcps range corresponding to 500 kcps throughput. This means collecting 5000 events per detector in the typical 10 ms period of spot delivery.

In PGT (and all other PG-based approaches to range verification) the number of registered events is larger than the number of ‘valid’ or ‘usable’ events. Event filtering is applied to suppress background and to select data comprising rather undisturbed range information. In case of PGT, only events with energy depositions in the detector between 3 and 7 MeV are considered to reduce the background caused by uncorrelated gamma rays, in particular annihilation radiation and 2.2 MeV gamma-ray emissions following neutron capture on ^1H. This energy cut rejects about 90 % of all events, leaving

[3] Scionix Holland B.V., https://scionix.nl/configurations-general/#tab-id-2
[4] Target Systemelektronik GmbH & Co. KG, http://target-sg.com/u100.html

only 500 usable events per spot and detector. This number can be gradually improved by raising the trigger threshold and fully exploiting the load capability of the detector itself, i.e. by shifting the bottleneck from electronic throughput to constraints given by the detector physics. However, a noticeable improvement of the statistics can only be achieved by using more detectors.

It must be emphasized that this limit is not due to an insufficient prompt-gamma production per spot but due to the finite event rates the detectors and electronics are able to process. In case of PGT, the interaction rates in the detectors could be raised by a factor of 4 or more just by reducing the detector distance from the isocenter to a about 20 cm, a distance often supposed in simulation studies. Then, however, neither detectors nor electronics could handle the load.

In conclusion, detector load and the bandwidth needed for data acquisition and processing are key parameters that must be considered in design studies of PG-based RVS. Neglecting this aspect could lead to investments in failing concepts.

3.3. Detector stability at strong and irregular load leaps

The count rate histograms in Figure 1 disclose another issue: Detection systems for prompt gamma rays are exposed to frequent, abrupt, irregular load leaps challenging the stability of detectors and electronics. Figure 5 exhibits count rate and Q-t histograms for a time section of the same measurement comprising selected energy layers of treatment field. The parameters Q and t mean the pulse charge (i.e., the raw energy) as delivered by the U100 spectrometer, approximately calibrated in MeV, and the time elapsed since start of data acquisition. The ridge at $Q \approx 0.5$ represents 511 keV annihilation gamma rays that are fully absorbed in the detector. Its slope changes at the same time as the beam is switched on or off. The load steps obviously induce retarded gain shifts [40] [41].

More detailed but not yet published investigations [42] confirm that the detector timing is affected as well. Timing effects seem, however, to be reasonably well correlated with the gain. This could allow correcting for time shifts by tracking the gain. Monitoring the position of the omnipresent 511 keV annihilation peak is meanwhile a standard procedure in PGT measurements anyway [40] [41] [29]. Such effects are not surprising for high-grade scintillators with ultimate light yield and short decay time combined with light readout by photomultiplier tubes (PMT). The light flood caused by the huge

flux of prompt gamma rays leading to considerable energy depositions in the crystal, eventually boosted by scattered protons crossing the scintillator, could easily provoke space charge effects in the tube, either in the photocathode or in the anode regions. Those could affect the PMT gain as well as the electron transit time and thus the timing. Note that excellent stabilization of anode and dynode voltages in view of the expected light load, as considered in the U100 design, is inevitable for such applications.

Figure 5

It is worth noting that similar effects could occur with other detector types or configurations as well. In case of the PGT detection systems, the gain and timing instabilities have been revealed in dedicated experiments with clinical beam intensities and time structures, and they have been observed in spite of stabilization means that prevented such drifts in less extreme operating conditions. We conclude that the stability of detector system to be used in RVS has to be proven at clinical modes of beam delivery; extrapolating laboratory experience to treatment conditions might be misleading.

4. Generalized approach to proton range verification based on prompt gamma-ray detection: Multi-feature range verification

Manufacturers of proton therapy facilities race towards higher beam currents and shorter treatment times. This is a question of economy (patient throughput, new accelerator types as synchrocyclotrons saving cost and space), safety and precision (reduction of dose blurring caused by unwanted motions of the patient, better treatment of moving tumors), as well as of convenience for the patients. Obviously, the rate and statistics problem inherent in prompt-gamma based range verification will not ease but sharpen in the coming years. Is there a way out?

As already mentioned, PGI and PGS make use of a tight event selection by (passive or electronic) collimation and filter criteria being part of the data analyses. This reduces the number of valid events but increases their ‘information content’, meaning their value for the respective analysis. An alternative strategy is measuring without collimation but compensating the lower ‘information content’ per event

by a much larger number of counts. PGT and PGPI follow this strategy. Both use, however, only one distinct feature for range reconstruction – detection time (PGT) or detection rate (PGPI). Best results could be expected if all aspects of information carried by every single gamma ray irrespective of their 'sharpness' would be considered in a comprehensive, generalized analysis, thus maximizing the overall information deployed for range assessment under the constraint of limited statistics. To illustrate this idea and to derive a corresponding hardware concept, we briefly discuss preliminary data obtained at OncoRay without going into much detail.

Figure 6 (left panel) shows a 2D histogram representing the energy-time correlation for gamma rays measured with a PGT detection unit during continuous irradiation of a beam-stopping polymethyl methacrylate (PMMA) target with 225 MeV protons delivered by the IBA Proteus®PLUS facility at OncoRay/UPTD. The exemplary data of excellent statistics were taken in a few-minutes run with stationary pencil beam just to illustrate the potential of combining energy and time analyses. E in the diagram means the energy deposition measured in the detector, t-t_{RF} the gamma-ray detection time with respect to the time reference, the accelerator RF signal. The time period just covers one micro-bunch cycle of the cyclotron. At the proton energy chosen, distinguished by lowest possible energy loss in the degrader, the system time resolution is in the 200-300 ps range [28]. The width of the timing peak is here essentially given by the proton stopping time in the target, the effect PGT is based on. This means the gamma-ray detection time is correlated with the penetration depth of the protons when generating the gamma rays. One could expect that a time cut is then equivalent with the kind of spatial collimation applied in PGS. In fact, the variation of distinct gamma line intensities along the time scale, observable by eye already in the 2D plot (left panel), becomes evident in time cuts as shown in the right panel. This suggests that the prompt gamma-ray timing and spectroscopy techniques, PGT and PGS, could be merged in a comprehensive data analysis simultaneously deploying time and energy information of PG events collected with an uncollimated detection system. Statistics and time resolution of a single-detector measurement for a single spot in a PBS treatment would of course be much worse than in Figure 6. However, one could use many detectors (instead of a bulky collimator), and develop methods of statistical data analysis to reconstruct the most probable prompt-gamma emission profile along the given beam track.

405 _____

406 Figure 6

407 _____

408

409 Detector segmentation is another aspect. In contrast to prompt gamma-ray imaging (PGI), the
410 'straight' methods of prompt gamma-ray spectroscopy (PGS), timing (PGT), and peak integration
411 (PGPI) do not a priori require detectors with spatial resolution. However, segmentation with individual
412 readouts and electronics per segment is very useful for two reasons:

413 1. Segmentation distributes the count rate from a single to multiple detectors and electronic
414 channels and thus multiplies the overall event rate that can be acquired. 3×3 arrays of
415 1.5×1.5×5 cm^3 scintillators, for instance, represent about the same active area, volume, and
416 scintillator mass as single ∅2"×2" crystals, but could tolerate an overall load (detector) and
417 provide an overall throughput (electronics) exceeding that of the monolithic detector by
418 about an order of magnitude. As mentioned in section 3.2, higher detector load could be
419 reached by reducing the detector-target distance.

420 2. Once the detector is segmented, additional information about the incidence direction of
421 incoming gamma rays and thus on the source position could be extracted from Compton-
422 scattering events sharing their energy depositions between two or more detector elements.
423 The corresponding technique has been introduced as Single-Plane Compton Imaging (SPCI)
424 [43].

425 SPCI builds on the idea of directional gamma radiation detectors (DGRD) as elaborated in [44] [45]
426 [46]. In contrast to usual Compton cameras, where individual scattering angles are determined event-
427 by-event, the DGRD extracts a *mean* incidence angle from 'conditional' energy spectra measured with
428 detectors arranged in a single plane. The condition is a coincident energy deposition in two (adjacent)
429 detector elements, preferably of a given sum energy, which is most likely due to Compton scattering in
430 one element followed by a second interaction in the other one. SPCI generalizes this concept [43]:
431 Maximum Likelihood Expectation Maximization (MLEM) algorithms disentangle the directional
432 information comprised in multiple conditional spectra acquired with a multi-pixel array for

reconstructing complex activity distributions. In case of PG-based range verification, the image space is basically reduced to a single dimension, the penetration depth along the beam track. This should facilitate a corresponding analysis. On the other hand, the statistics of usable events is very restricted. Though Compton scattering dominates over photoabsorption and pair production in the PG energy range, not every interaction leads to energy depositions in multiple detector segments. According to explorative simulations [47], the corresponding fraction is expected to reach a few up to about twenty percent or even more, depending on the detector geometry, granularity, and filter criteria (sum energy cut, number of the segments involved, energy thresholds in the detector segments, etc.). In combination with the gain in load capability one could, however, anticipate a number of potential SPCI events as high as the number of usable events in case of PGT with unsegmented detectors.

The usability of the DGRD principle, so far only considered for energies below 1-2 MeV, has meanwhile been confirmed for prompt gamma rays of 4.45 MeV [47]. Two pairs of PGT detection units, arranged head-to-head with axes parallel to a proton beam penetrating a beam-stopping PMMA target, registered prompt gamma rays produced by a stationary proton pencil beam. Coincidences between adjacent 'upstream' and 'downstream' detectors were analyzed, considering only events with corresponding energy depositions E_u and E_d above 511 keV and a sum energy $E_{sum} = E_u + E_d$ around 4.45 MeV. Mean energies $\langle E_u \rangle$ and $\langle E_d \rangle$ were computed for the conditional single-detector spectra tagged with the coincidence and filter conditions. Finally, a Figure of Merit (FOM) was introduced as

$$FOM = \frac{\langle E_d \rangle - \langle E_u \rangle}{E_{sum}}$$

Figure 7 shows a sketch of the setup and presents FOM as a function of the target position for the exemplary proton energy of 90 MeV. It is evident that the target position, related to the 'average location' of the prompt-gamma source, is retrievable from FOM. This justifies the assumption that SPCI could contribute to the reconstruction of the prompt-gamma emission profiles along the beam axis. We have to note that the data presented comprise about 1000 times the statistics obtainable from a single PBS spot. Furthermore, the results turned out to be very sensitive to detector gain drifts. Actually a dedicated calibration procedure took care for an almost negligible calibration uncertainty (translating to corresponding virtual gain stability) of around 0.1 % [47].

Figure 7

Future systems for PG-based range verification could therefore consist of multiple detector segments, distinguished by excellent energy and time resolution, arranged side-by-side, each provided with an individual electronics channel performing high-throughput time and energy spectroscopy. Detection time, sum energy, and energy sharing between detector segments had to be measured for every detected gamma ray. A comprehensive data analysis, based e.g. MLEM formalisms, would consider these complementary aspects for reconstructing the most probable gamma-ray emission profile along the pencil beam track, i.e., for determining the range of an individual PBS spot.

5. Detectors for multi-feature range verification systems

This concept, below referred to as multi-feature range verification system (MRVS), combines PGS, PGT, and PGI (in the form of SPCI) in a single detection system. Though corresponding data analysis schemes have not yet been developed, the hardware to be used can already be sketched. The key parameters derived and discussed below are summarized in Table 2.

5.1. Detector construction

SPCI requires the system to consist of detector pixels with individual readouts. For reasons of flexibility and scalability, a modular construction is advisable. At first glance, detector modules developed for PET-MR (see e.g. [48]) look promising for SPCI as well as for PGT. They usually consist of LSO or LYSO scintillator pixels read out with silicon photomultipliers (SiPM) or avalanche photodiodes (APD). Their time resolution is excellent. However, the relatively high internal activity of these scintillators, caused by β^- decays of ^{176}Lu accompanied by gamma-ray cascades from of the excited daughter nuclide ^{176}Hf, would generate many true β–γ coincidences in adjacent detector pixels contaminating the useful SPCI (i.e., Compton-scattering) events. Furthermore, the mediocre energy resolution of these crystals would not be sufficient for PGS.

Nevertheless it is obvious to translate the construction principle of PET-MR detectors to an MRVS. This means using pixels of fast and bright scintillator materials, distinguished by excellent linearity and negligible internal activity, providing them with individual Si-based light sensors, and arranging a reasonable number of such pixels in an array forming an MRVS detection module. The size of the scintillator pixels has to be chosen as a compromise between cost (strongly affected by the number of readout channels) and reasonable granularity. The pixel depth should fit with the absorption length for 4-5 MeV gamma rays. Considering the active area of available light sensors and an acceptable depth-to-base ratio, pixel bases of 6-10 mm and pixel depths of 3-5 cm seem reasonable cornerstones.

5.2. Energy resolution

The energy resolution of MRVS pixels must be good enough for PGS. Reference [25] states a resolution of 1.3 % at 6.1 MeV gamma-ray energy achieved with the ∅2”×3” $LaBr_3$:Ce detectors of a clinical PGS system at clinical dose rates. PGT detection units with ∅2”×2” $CeBr_3$ detectors exhibited 3.5 %, 2.5 %, and 1.2 % energy resolution at 1.3 MeV, 2.5 MeV, and 6.1 MeV, respectively [41] [49]. These data can be considered as benchmark for MRVS pixels.

5.3. Time resolution

Requirements for time resolution are equivalent with those resulting from PGT. We have to consider that the time resolution of PGT *systems* is basically limited by the finite width of the proton micro-bunches [28]. At first glance, one could suppose a start detector with ultimate time resolution and rate capability providing an individual timing signal for every proton would overcome this limitation. However, the finite proton stopping time in the target is much larger than time intervals between consecutive protons crossing the hypothetic detector. (Note that, at clinical beam currents, this would hold even if the beam was not bunched but continuous.) Consequently the spread of the period between proton passage and correlated prompt gamma-ray emission, or between proton passage and correlated gamma-ray detection, is much larger than the average period between consecutive proton detections. Therefore a single gamma ray could never be attributed to a distinct proton. In other words: The proton bunch signal is the only time reference on hand. A start detector could in fact be useful for improving the time reference for proton *bunches*, but not for providing distinct time references for single protons and the corresponding prompt gamma rays.

At UPTD the minimum proton bunch width is about 250 ps (FWHM), measured at a relatively short beamline at maximum proton energy (225 MeV). For energies between 90 and 160 MeV a much larger bunch width was observed, ranging from 1 to 2 ns, which could even be worsened by a longer beamline [28]. The PGT detection systems were designed to essentially not affect the system time resolution, even in the best case of maximum proton energy. This led to a required (and later on proven) time resolution of ~250 ps in the energy range of prompt gamma-rays [37]. This requirement could, however, be relaxed in view of clinical applications.

5.4. Tolerable detector load

A benchmark for load tolerance of the detectors and electronics throughput is set by the available PGT detection systems [37]. Lower load and throughput limits per channel could be acceptable since the envisaged segmentation in relatively small pixels allowed increasing the overall detection rate even at reduced load per channel.

5.5. Gain stability

The SPCI technique relies on the detection and quantification of small mean shifts and shape variations of energy spectra measured with different detector pixels. Such variations could be feigned by gain instabilities of individual detectors. As already mentioned, the clear correlation between FOM and source position shown in Figure 7 could only be revealed by using an elaborated calibration procedure correcting for potential gain shifts at an accuracy level of 0.1%. This calibration is based on the mutual matching of straight energy spectra obtained with the individual detectors [47] [51] and works well because of the good statistics of these measurements.

In MRVS, gain fluctuations due to load leaps may occur at a time scale of milliseconds, see Figure 5. Active gain stabilization seems unavoidable. A recent approach, based on a quantification of ‘noise’ caused by statistically fluctuating single-photoelectron contributions to the detector signal [52], might provide the necessary stability at time scales in the sub-second range.

5.6. Challenge and potential approach

Each of the characteristics listed in Table 2 has already been reached with detector systems at hand. However, achieving *simultaneous* compliance with *all* requirements is difficult.

It seems an obvious approach to rely on the construction scheme and the SiPM light sensors of recent PET-MR detectors but to replace the LSO or LYSO crystals by $CeBr_3$ or $LaBr_3$:Ce. The high light yield of these scintillators, however, combined with the high energies of prompt gamma rays, conflicts with the limited number of microcells comprised in a SiPM. Prompt gamma rays of 4-6 MeV could easily generate $2\text{-}4\times10^5$ scintillation photons per pulse and thus drive every commercial SiPM into saturation. Though saturation effects can be corrected for, they could seriously deteriorate the energy resolution just in the energy range most relevant for PGS. Careful measurements comparing the energy resolution of $CeBr_3$, NaI:Tl, and CsI:Tl scintillators if read out with silicon photomultipliers or common photomultiplier tubes confirmed the clear disadvantage of SiPM in case of the fast and bright $CeBr_3$ but even for the much slower NaI:Tl crystals in the energy range up to 6.1 MeV [53]. Reducing the light collection efficiency is not an option since this would raise the statistical contribution to energy resolution. Another weak point is the sensitivity of SiPM gains to external factors as bias voltage and ambient temperature. Though gain stabilization at the percent level can be achieved by temperature monitoring and voltage control, reaching the 0.1% mark might be a problem.

In view of the high gamma-ray energies of interest, light sensors without internal gain could be a feasible alternative. PIN photodiodes (PD) have been used in gamma-ray spectroscopy with scintillators, for instance with CsI:Tl, for decades. The energy resolution of a scintillator-PD combination suffers from noise contributions of diode and preamplifier. That is why PD readout is not competitive for spectroscopy in the low-energy range of common radioactive sources. On the other hand, photodiodes are distinguished by outstanding detection efficiency for optical photons (quantum efficiency) by far exceeding the quantum efficiency of PMTs or the photodetection efficiency of SiPMs. The different scaling of noise and statistical contributions to the energy resolution with growing photon number (i.e. increasing energy deposition) leads to an advantage of PD readout if compared with PMT readout for energies above 1-2 MeV. This was demonstrated in corresponding measurements with $LaBr_3$:Ce crystals [54]. $CeBr_3$ or $LaBr_3$:Ce detectors with photodiode readout are thus expected to be compatible with the energy resolution and gain stability criteria given in Table 2. Critical points are the achievable time resolution and load tolerance.

Developing suitable detection systems for multi-feature range verification system is obviously not a straightforward exercise but a challenge. Recent efforts at OncoRay and HZDR are focused on comparative studies of readout options considering realistic treatment conditions.

6. Summary and conclusions

Range verification of proton beams in radio-oncological treatments is a challenge many research groups have been engaged in. The clinical environment and workflow as well as time structure and intensities of therapeutic beams define constraints for range verification systems that are not always considered in depth in simulation studies or system designs. This could lead to misguided investments, also in terms of wasted effort and manpower.

The paper therefore analyzed and discussed general constraints for range verification systems based on the detection of prompt gamma rays. Range verification for a single, strong pencil beam spot at clinical rate of dose delivery is set as benchmark. The short duration of a single spot delivery, the immense gamma-ray production rate during delivery, the finite load tolerance of detectors, and electronic throughput limits were identified as major factors limiting the event statistics that can be collected for a single pencil beam spot. For Compton cameras and other systems based on coincidence measurements, rate and fraction of random coincidences may restrict the applicable overall detection efficiency and thus further reduce the achievable statistics. Note that in practice few pencil beam spots could be summed up to lower range uncertainties on the expense of spatial resolution. This means, however, a gradual but not a principal relief. Reference to a single spot is, to our opinion, a useful benchmark to compare systems of different designs.

In conclusion a generalized concept for prompt-gamma based range verification is proposed. The gamma rays should be measured with scintillation detector modules consisting of multiple pixels with individual readouts. This would increase the number of prompt gamma rays that can be detected per pencil beam spot, and would allow extracting as much information as possible from every gamma-ray event in order to assess the range of clinical proton beams with ultimate precision. Though similar detector modules have been developed for applications as PET-MR, the envisaged measurement of prompt gamma rays is much more demanding with respect to dynamic range, energy resolution, load acceptance, and stability.

It is worth noting that such detection modules could also be used for measuring annihilation gamma rays, even in parallel to the prompt gamma rays produced during dose delivery. This opens the way for additional in-beam PET imaging, supposed that multiple detector modules are arranged in PET-compatible geometry.

Acknowledgments

The authors would like to thank Christian Richter, Steffen Löck (Helmholtz-Zentrum Dresden – Rossendorf, Institute of Radiooncology – OncoRay, Dresden, Germany), Julien Smeets, and Johannes Petzoldt (IBA Ion Beam Applications S.A., Lovain-la-Neuve, Belgium) for helpful discussions that motivated writing of and provided substantial information for this paper.

References

[1] Particle Therapy Co-Operative Group (PTCOG): Particle therapy facilities in operation. Updated in April 2018. https://www.ptcog.ch/index.php/facilities-in-operation

[2] J.S. Loeffler and M. Durante, Charged particle therapy—optimization, challenges and future directions, Nature Reviews Clinical Oncology 10 (2013) 411–424. https://doi.org/10.1038/nrclinonc.2013.79

[3] A.C. Knopf and A. Lomax, In vivo proton range verification: a review, Phys. Med. Biol. 58 (2013) R131. https://doi.org/10.1088/0031-9155/58/15/R131

[4] K. Parodi, On- and off-line monitoring of ion beam treatment, Nucl. Instrum. Meth. A 809 (2016) 113. https://doi.org/10.1016/j.nima.2015.06.056

[5] W. Enghardt, P. Crespo, F. Fiedler, R. Hinz, K. Parodi, J. Pawelke, F. Pönisch, Charged hadron tumour therapy monitoring by means of PET, Nucl. Instrum. Meth. A 525 (2004) 284. http://dx.doi.org/10.1016/j.nima.2004.03.128

[6] A. Knopf, K. Parodi, T. Bortfeld, H.A. Shih and H. Paganetti, Systematic analysis of biological and physical limitations of proton beam range verification with offline PET/CT scans, Phys. Med. Biol. 54 (2009) 4477. https://doi.org/10.1088/0031-9155/54/14/008

[7] F. Pennazio, G. Battistoni, M.G. Bisogni, N. Camarlinghi, A. Ferrari, V. Ferrero, E. Fiorina, M. Morrocchi, P.R. Sala, G. Sportelli, R. Wheadon and P. Cerello, Carbon ions beam therapy monitoring with the INSIDE in-beam PET, Phys. Med. Biol. (2018) *in press*, https://doi.org/10.1088/1361-6560/aacab8

[8] C.H. Min, C.H. Kim, M.Y. Youn, J.W. Kim, Prompt gamma measurements for locating the dose falloff region in the proton therapy, Appl. Phys. Lett. 89 (2006) 183517. http://dx.doi.org/10.1063/1.2378561

[9] K.S. Seo C.H. Kim, J.W. Kim, Comparison of Titanium Hydride (TiH_2) and Paraffin as Neutron Moderator Material in a Prompt Gamma Scanning System, J. Korean Phys. Soc. 48 (2006) 855. http://www.jkps.or.kr/journal/view.html?uid=7726&vmd=Full

[10] J. Smeets, F. Roellinghoff, D. Prieels, F. Stichelbaut, A. Benilov, P. Busca, C. Fiorini, R. Peloso, M. Basilavecchia, T. Frizzi, J.C. Dehaes and A. Dubus, Prompt gamma imaging with a slit camera for real-time range control in proton therapy, Phys. Med. Biol. 57 (2012) 3371. https://doi.org/10.1088/0031-9155/57/11/3371

[11] M. Pinto et al., D. Dauvergne, N. Freud, J. Krimmer, J.M. Letang, C. Ray, F. Roellinghoff, E. Testa, Design optimisation of a TOF-based collimated camera prototype for online hadrontherapy monitoring, Phys. Med. Biol. 59 (2014) 7653. https://doi.org/10.1088/0031-9155/59/24/7653

[12] I. Perali, A. Celani, L. Bombelli, C. Fiorini, F. Camera, E. Clementel, S. Henrotin, G. Janssens, D. Prieels, F. Roellinghoff, J. Smeets, F. Stichelbaut and F Vander Stappen, Phys Med Biol. 59 (2014) 5849. https://doi.org/10.1088/0031-9155/59/19/5849

[13] C. Richter, G. Pausch, S. Barczyk, M. Priegnitz, I. Keitz, J. Thiele, J. Smeets, F. Vander Stappen, L. Bombelli, C. Fiorini, L. Hotoiu, I. Perali, D. Prieels, W. Enghardt, and M. Baumann, First clinical application of a prompt gamma based in vivo proton range verification system, Radiother. Oncol. 118 (2016) 232. http://dx.doi.org/10.1016/j.radonc.2016.01.004

[14] Y. Xie, E.H. Bentefour, G. Janssens, J. Smeets, F. Vander Stappen, L. Hotoiu, L. Yin, D. Dolney, S. Avery, F. O'Grady, D. Prieels, J. McDonough, T.D. Solberg, R.A. Lustig, A. Lin, B.K.K. Teo, Prompt Gamma Imaging for In Vivo Range Verification of Pencil Beam Scanning Proton Therapy, Int. J. Radiat. Oncol. Biol. Phys. 99 (2017) 210. https://doi.org/10.1016/j.ijrobp.2017.04.027

[15] L. Nenoff, M. Priegnitz, G. Janssens, J. Petzoldt, P. Wohlfahrt, A. Trezza, J. Smeets, G. Pausch, C. Richter, Sensitivity of a prompt-gamma slit-camera to detect range shifts for proton treatment verification, Radiother. Oncol. 125 (2017) 534. https://doi.org/10.1016/j.radonc.2017.10.013

[16] P.G. Thirolf, S. Aldawood, M. Böhmer, J. Bortfeldt, I. Castelhano, G. Dedes, F. Fiedler, R. Gernhäuser, C. Golnik, S. Helmbrecht, F. Hueso-González, H. v.d. Kolff, T. Kormoll, C. Lang, S. Liprandi, R. Lutter, T. Marinšek, L. Maier, G. Pausch, J. Petzoldt, K. Römer, D. Schaart and K. Parodi, A Compton camera prototype for prompt gamma medical imaging, EPJ Web of Conferences 117 (2016) 05005. https://doi.org/10.1051/epjconf/201611705005

[17] J. Krimmer, J.-L. Ley, C. Abellan, J.-P. Cachemiche, L. Caponetto, X. Chen, M. Dahoumane, D. Dauvergne, N. Freud, B. Joly, D. Lambert, L. Lestand, J.M. Létang, M. Magne, H. Mathez, V. Maxim, G. Montarou, C. Morel, M. Pinto, C. Ray, V. Reithinger, E. Testa, Y. Zoccarato, Development of a Compton camera for medical applications based on silicon strip and scintillation detectors, Nucl. Instrum. Meth. A 787 (2015) 98. https://doi.org/10.1016/j.nima.2014.11.042

[18] M. McCleskey, W. Kaye, D.S. Mackin, S. Beddar, Z.He, J.C. Polf, Evaluation of a multistage CdZnTe Compton camera for prompt γ imaging for proton therapy, Nucl. Instrum. Meth. A 785 (2015) 163. http://dx.doi.org/10.1016/j.nima.2015.02.030

[19] G. Llosá, M. Trovato, J. Barrio, A. Etxebeste, E. Muñoz, C. Lacasta, J.F. Oliver, M. Rafecas, C. Solaz and P. Solevi, First Images of a Three-Layer Compton Telescope Prototype for Treatment Monitoring in Hadron Therapy, Front. Oncol. 6 (2016) 14. https://doi.org/10.3389/fonc.2016.00014

[20] F. Hueso-González, G. Pausch, J. Petzoldt, K.E. Römer, and W. Enghardt, Prompt Gamma Rays Detected With a BGO Block Compton Camera Reveal Range Deviations of Therapeutic Proton Beams, IEEE Trans. Rad. Plasma Med. Sci. 1 (2017) 76. https://doi.org/10.1109/TNS.2016.2622162

[21] C. Golnik, D. Bemmerer, W. Enghardt, F. Fiedler, F. Hueso-González, G. Pausch, K. Römer, H. Rohling, S. Schöne, L. Wagner, and T. Kormoll, Tests of a Compton imaging prototype in a monoenergetic 4.44MeV photon field — a benchmark setup for prompt gamma-ray imaging devices, J. Instrum. 11 (2016) P06009. http://dx.doi.org/10.1088/1748-0221/11/06/P06009

[22] H. Rohling, M. Priegnitz, S. Schoene, A. Schumann, W. Enghardt, F. Hueso-González, G. Pausch and F. Fiedler, Requirements for a Compton camera for *in vivo* range verification of proton therapy, Phys. Med. Biol. 62 (2017) 2795. https://doi.org/10.1088/1361-6560/aa6068

[23] E. Draeger, D. Mackin, S. Peterson, H. Chen, S. Avery, S. Beddar and J C Polf, 3D prompt gamma imaging for proton beam range verification, Phys. Med. Biol. 63 (2018) 035019. https://doi.org/10.1088/1361-6560/aaa203

[24] J.M. Verburg and J. Seco, Proton range verification through prompt gamma-ray spectroscopy, Phys. Med. Biol. 59 (2014) 7089. https://doi.org/10.1088/0031-9155/59/23/7089

[25] F. Hueso González, M. Rabe, T. Ruggieri, T. Bortfeld, J.M. Verburg, A full-scale clinical prototype for proton range verification using prompt gamma-ray spectroscopy, paper submitted to Phys. Med. Biol. (2018), under review

[26] C. Golnik, F. Hueso-González, A. Müller, P. Dendooven, W. Enghardt, F. Fiedler, T. Kormoll, K. Roemer, J. Petzoldt, A. Wagner and G. Pausch, Range assessment in particle therapy based on prompt γ-ray timing measurements, Phys. Med. Biol. 59 (2014) 5399. http://dx.doi.org/10.1088/0031-9155/59/18/5399

[27] F. Hueso González, W. Enghardt, F. Fiedler, C. Golnik, G. Janssens, J. Petzoldt, D. Prieels, M. Priegnitz, K.E. Römer, J. Smeets, F. Vander Stappen, A. Wagner, and G. Pausch, First test of the prompt gamma ray timing method with heterogeneous targets at a clinical proton therapy facility, Phys. Med. Biol. 60 (2015) 6247. http://dx.doi.org/10.1088/0031-9155/60/16/6247

[28] J. Petzoldt, K.E. Roemer, W. Enghardt, F. Fiedler, C. Golnik, F. Hueso-González, S. Helmbrecht, T. Kormoll, H. Rohling, J. Smeets, T. Werner and G Pausch, Characterization of the microbunch time

structure of proton pencil beams at a clinical treatment facility, Phys. Med. Biol. 61(2016) 2432. https://doi.org/10.1088/0031-9155/61/6/2432

[29] T. Werner, J. Berthold, F. Hueso-González, T. Kögler, J. Petzoldt, K. Roemer, C. Richter, A. Rinscheid, A. Straessner, W. Enghardt and G. Pausch, Processing of prompt gamma-ray timing data for precise proton range measurements at a clinical beam delivery, paper submitted to Phys. Med. Biol. (2018), under review.

[30] J. Krimmer, G. Angellier, L. Balleyguier, D. Dauvergne, N. Freud, J. Hérault, J.M. Létang, H. Mathez, M. Pinto, E. Testa, and Y. Zoccarato, A Cost-Effective Monitoring Technique in Particle Therapy via Uncollimated Prompt Gamma Peak Integration, Appl. Phys. Lett. 110 (2017) 154102. https://doi.org/10.1063/1.4980103

[31] J. Krimmer, D. Dauvergne, J.M. Létang, É. Testa, Prompt-gamma monitoring in hadrontherapy: A review, Nucl. Instrum. Meth. A 878 (2018) 58. https://doi.org/10.1016/j.nima.2017.07.063

[32] P. Farace, R. Righetto and A. Meijers, Pencil beam proton radiography using a multilayer ionization chamber, Phys. Med. Biol. 61 (2016) 4078. http://dx.doi.org/10.1088/0031-9155/61/11/4078

[33] M. Yamaguchi, Y. Nagao, K. Ando, S. Yamamoto, M. Sakai, R.K. Parajuli, K. Arakawa and N. Kawachi, Imaging of monochromatic beams by measuring secondary electron bremsstrahlung for carbon-ion therapy using a pinhole X-ray camera, Phys. Med. Biol. 63 (2018) 045016. https://doi.org/10.1088/1361-6560/aaa17c

[34] M. Yamaguchi, Y. Nagao, K. Ando, S. Yamamoto, T. Toshito, J. Kataoka, N. Kawachi, Secondary-electron-bremsstrahlung imaging for proton therapy, Nucl. Instrum. Meth. A 833 (2017) 199. https://doi.org/10.1016/j.nima.2016.07.034

[35] S.K. Patch, M. Kireeff Covo, A. Jackson, Y.M. Qadadha, K.S. Campbell, R.A. Albright, P. Bloemhard, A.P. Donoghue, C.R. Siero, T.L. Gimpel, S.M. Small, B.F. Ninemire, M.B. Johnson and L. Phair, Thermoacoustic range verification using a clinical ultrasound array provides perfectly co-registered overlay of the Bragg peak onto an ultrasound image, Phys. Med. Biol. 61(2016) 5621. https://doi.org/10.1088/0031-9155/61/15/5621

[36] S. Lehrack, W. Assmann, D. Bertrand, S. Henrotin, J. Herault, V. Heymans, F. Vander Stappen, P.G Thirolf, M. Vidal, J. Van de Walle and K. Parodi, Submillimeter ionoacoustic range determination for protons in water at a clinical synchrocyclotron, Phys. Med. Biol. 62(2017) L20. https://doi.org/10.1088/1361-6560/aa81f8

[37] G. Pausch, J. Petzoldt, M. Berthel, W. Enghardt, F. Fiedler, C. Golnik, F. Hueso-González, R. Lentering, K. Römer, K. Ruhnau, J. Stein, A. Wolf, and T. Kormoll, Scintillator-Based High-Throughput Fast Timing Spectroscopy for Real-Time Range Verification in Particle Therapy, IEEE Trans. Nucl. Sci. 63 (2016) 664. http://dx.doi.org/10.1109/TNS.2016.2527822

[38] F. Fiedler, U. Dersch, C. Golnik, T. Kormoll, A. Müller, H. Rohling, S. Schöne and W. Enghardt, The Use of Prompt γ-rays for in-vivo Dosimetry at Therapeutic Proton and Ion Beams, 2011 IEEE Nuclear Science Symposium Conference Record, 4453. https://doi.org/10.1109/NSSMIC.2011.6152493

[39] G.F. Knoll, Radiation Detection and Measurement, Fourth Edition, John Wiley & Sons, 2010, Chapter 17, page 659. ISBN: 978-0-470-13148-0

[40] A. Rinscheid, J. Berthold, W. Enghardt, C. Golnik, F. Fiedler, F. Hueso-Gonzáles, T. Kormoll, R. Lentering, J. Petzoldt, K. Römer, K. Ruhnau, J. Stein, T. Werner, A. Wolf, D. Reichert, G. Pausch, Characterization of a fast timing and energy spectroscopy system for real-time range verification in particle therapy, paper N29-20 presented at the 2016 IEEE Nuclear Science Symposium and Medical Imaging Conference in Strasbourg, France, Oct. 29 – Nov. 06, 2016.

[41] A. Rinscheid, Steps towards the clinical implementation of a digital spectrometer system for range verification in proton therapy, Master Thesis, Martin-Luther-Universität Halle / Technische Universität Dresden / OncoRay, 2016

[42] C. Müller, Untersuchung des Verhaltens eines Detektorsystems unter Lastwechseln im Hinblick auf die Prompt Gamma-Ray Timing Methode, Master Thesis, Technische Universität Dresden / OncoRay, 2017

[43] G. Pausch, C. Golnik, A. Schulz and W. Enghardt, A Novel Scheme of Compton Imaging for Nuclear Medicine, 2016 IEEE Nuclear Science Symposium, Medical Imaging Conference and Room-Temperature Semiconductor Detector Workshop (NSS/MIC/RTSD), Conference Record. https://doi.org/10.1109/NSSMIC.2016.8069921

[44] G. Kraft, W. Enghardt, T. Wuerschig, Detector Assembly for Detecting Radiation with Angular Resolution and Method for Operating Said Assembly, US Patent No. 8030617. Filed: Jun. 18, 2007; Granted: Oct. 04, 2011

[45] A. Gueoguiev, J. Preston, L. Hoy, G. Pausch, C.-M. Herbach and J. Stein, A Novel Method to Determine the Directionality of Radiation Sources with Two Detectors Based on Coincidence Measurements, 2010 Nuclear Science Symposium, Medical Imaging Conference and Room-Temperature Semiconductor Detector Workshop (NSS/MIC/RTSD), Conference Record. https://doi.org/10.1109/NSSMIC.2010.5874031

[46] A. Gueoguiev, G. Pausch, C.-M. Herbach, L. Hoy, Directional gamma radiation detector system, US Patent No. 8299441. Filed: Aug. 5, 2010; Granted: Oct. 30, 2012.

[47] J. Berthold, Single Plane Compton Imaging for Range Verification in Proton Therapy- A Proof-of-Principle Study, Master Thesis, Technische Universität Dresden / OncoRay, 2018

[48] P.J. Slomka, T. Pan, and G. Germano, Recent Advances and Future Progress in PET Instrumentation, Seminars in Nuclear Medicine 46 (2016) 5. https://doi.org/10.1053/j.semnuclmed.2015.09.006

[49] E. Berg and S.R. Cherry, Innovations in Instrumentation for Positron Emission Tomography, Seminars in Nuclear Medicine 48 (2018) 311. https://doi.org/10.1053/j.semnuclmed.2018.02.006

[50] F. Buch, Messung des Emissionsspektrums prompter Photonen bei der Bestrahlung homogener Targets mit Protonen, Master Thesis, Technische Universität Dresden / OncoRay, 2018

[51] Y. Kong, G. Pausch, K. Römer, A. Kreuels, C.-M. Herbach, M. Neuer, R. Lentering, and J. Stein, Linearization of Gamma Energy Spectra in Scintillator-Based Commercial Instruments, IEEE Trans. Nucl. Sci. 57 (2010) 1430. https://doi.org/10.1109/TNS.2009.2033684

[52] J. Stein, A. Kreuels,Y. Kong, R. Lentering, K. Ruhnau, F. Scherwinski, A. Wolf, Experiment and modeling of scintillation photon-counting and current measurement for PMT gain stabilization, Nucl. Instrum. Meth. A 782 (2015) 20. https://doi.org/10.1016/j.nima.2015.01.101

[53] M. Grodzicka-Kobylka, T. Szczesniak, M. Moszyński, L. Swiderski, M. Szawłowski, Silicon photomultipliers in scintillation detectors used for gamma ray energies up to 6.1 MeV, Nucl. Instrum. Meth. A 874 (2017) 137. https://doi.org/10.1016/j.nima.2017.08.031

[54] M. Moszyński, C. Plettner, A. Nassalski, T. Szczesniak, Ł. Swiderski, A. Syntfeld-Kazuch, W. Czarnacki, G. Pausch, J. Stein, A. Niculae, and H. Soltau, A Comparative Study of Silicon Drift Detectors With Photomultipliers, Avalanche Photodiodes and PIN Photodiodes in Gamma Spectrometry With $LaBr_3$ Crystals, IEEE Trans. Nucl. Sci. 56 (2009) 1006. https://doi.org/10.1109/TNS.2008.2005110

777

778 Table 1.

779 Key parameters of pencil-beam scanning (PBS) treatments at the IBA Proteus®PLUS facility at the University
780 Proton Therapy Dresden (UPTD)

781

Parameter	Value			
	general	per microbunch	per PBS spot	per second
Cyclotron RF	106 MHz			
Microbunch separation	9.6 ns			
Beam current[a]	≈2 nA			
Prompt gamma production yield per proton [10][38]	0.1 – 0.3			
Number of protons[a]		100	10^8	10^{10}
Number of prompt gamma rays[a]		10-30	$1\text{-}3\times10^7$	$1\text{-}3\times10^9$

782 [a]Typical values during delivery of strong (distal) pencil beam spots.

783

Table 2.

Intended key parameters of detectors to be used for range verification based on prompt gamma rays according to the generalized multi-feature range verification concept

Parameter	Value
Approximate size	1 cm^2 × 3…5 cm
Tolerable detector load	1 Mcps [a]
Electronic throughput at tolerable detector load	500 kcps [a]
Energy resolution	3.5% @ 1.3 MeV [a]
	2.5% @ 2.5 MeV [a]
	1.2-1.3% @ 6.1 MeV [a,b]
Time resolution (CRT)	250 ps @ 4.5 MeV [a]
Gain stability	0.1 % [c]

[a] Values achieved with PGT detection units [37] [40] [41] [49]

[b] Resolution stated in [25]

[c] Gain accuracy achieved by means of a dedicated calibration procedure [47]

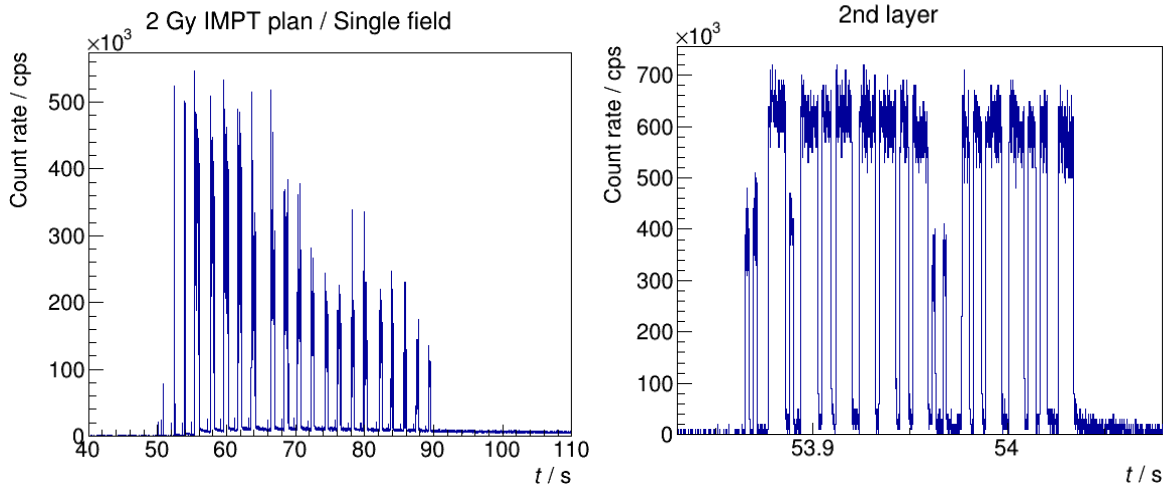

Figure 1. Count rate (throughput at 1 μs dead time per event) measured with a PGT detection unit [37] during delivery of a realistic IMPT treatment field to an anthropomorphic head phantom. Parameter t denotes time elapsed since start of data acquisition. The histograms disclose the time structure of dose delivery: Energy layers are separated by few-seconds breaks for beam-energy switching (left panel). Each layer is structured in distinct PBS spots of few-milliseconds duration (right panel). Note the extreme load variations at a millisecond time scale.

803

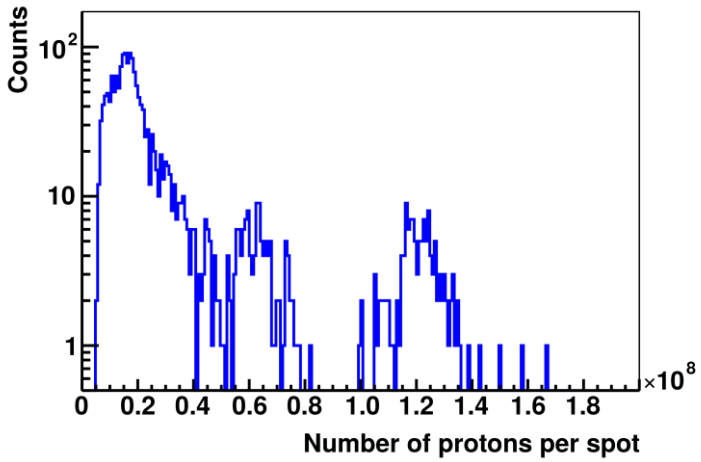

804

805

806 Figure 2. Distribution of PBS spot strengths (in terms of protons per spot) of the IMPT treatment
807 field referred to in the text and in Figure 1.

808

809

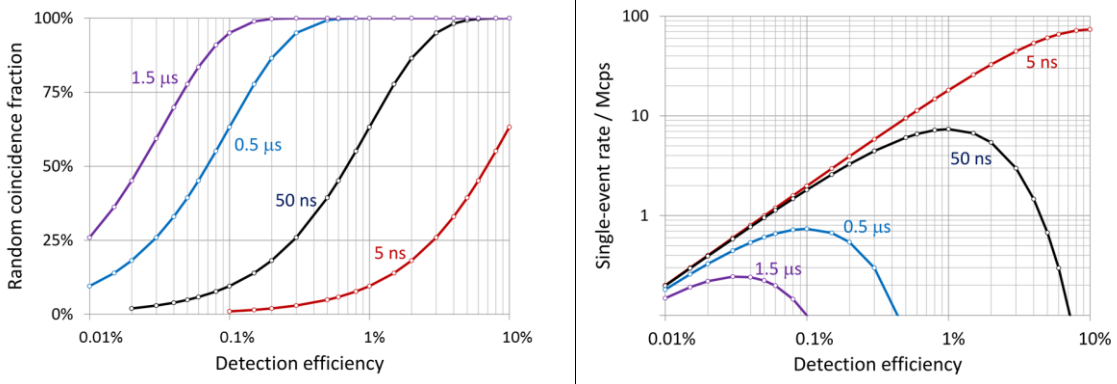

Figure 3. Minimum random coincidence fraction (left panel) and maximum true coincidence rate (right panel) of a Compton camera as function of system detection efficiency and coincidence time resolution. A prompt-gamma production rate of 2×10^{9} s^{-1} was assumed, which corresponds to realistic treatment conditions (see Table 1).

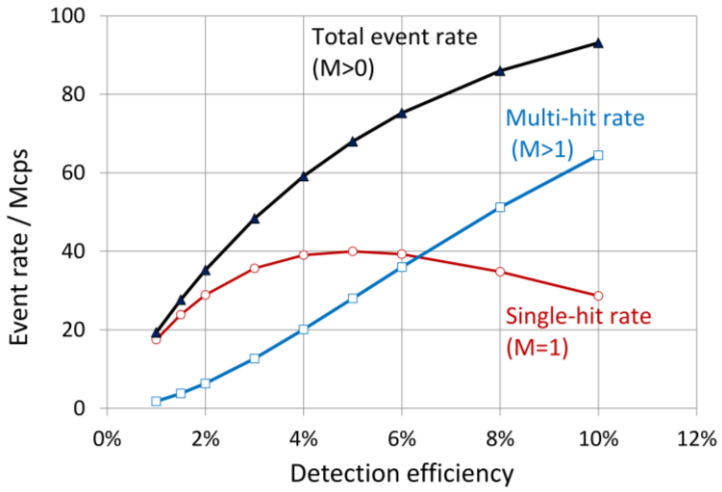

Figure 4. Single- and multi-hit rates compared with the total event rate as function of the system detection efficiency. A bunch repetition frequency of 106 MHz and an (average) number of 20 prompt gamma rays produced per bunch were assumed in accordance with Table 1. Multi-hits are caused by simultaneous detections of two or more prompt gamma rays of the same micro-bunch. Their fraction increases with the system detection efficiency on the expense of single-hit detections, finally leading to decreasing single-hit rate.

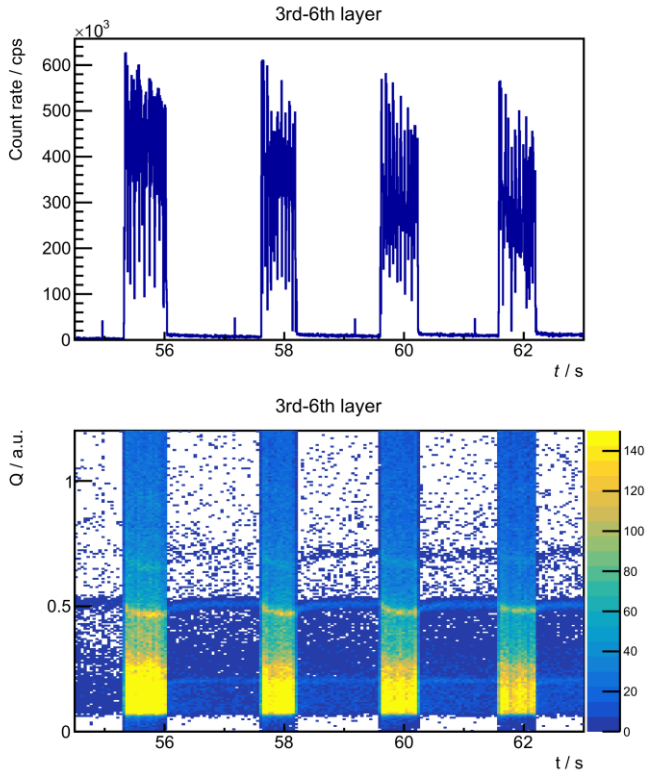

Figure 5. Count rate (upper graph) and Q-t histograms (lower graph) for the 3rd to 6th layer of the IMPT treatment field referred to in the text and in Figure 1. The parameters Q and t mean the pulse charge (raw energy without gain drift correction, approximately calibrated in MeV), and the time elapsed since start of data acquisition. Retarded gain shifts caused by load leaps are clearly visible in the ridge representing 511 keV annihilation gamma rays absorbed in the detector ($Q \approx 0.5$).

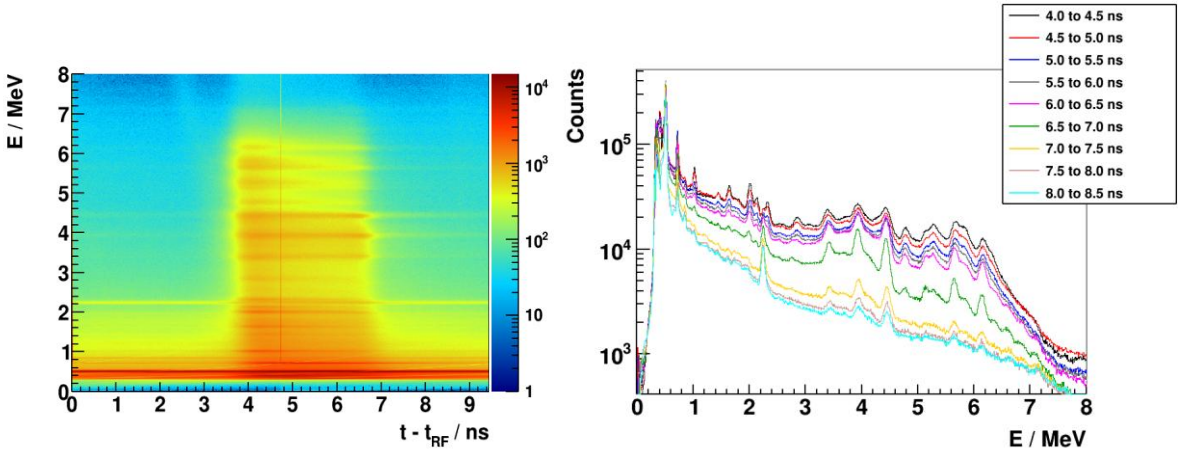

Figure 6. Energy-time histogram of gamma rays emitted from a PMMA target during irradiation with a stationary 225 MeV proton beam (left panel), measured with a PGT detection unit comprising a ∅2”×2” $CeBr_3$ scintillation detector. Time cuts in these data correspond to spatial collimation; they disclose the variation of line intensities with the penetration depth of the protons as deployed for PGS (right panel).

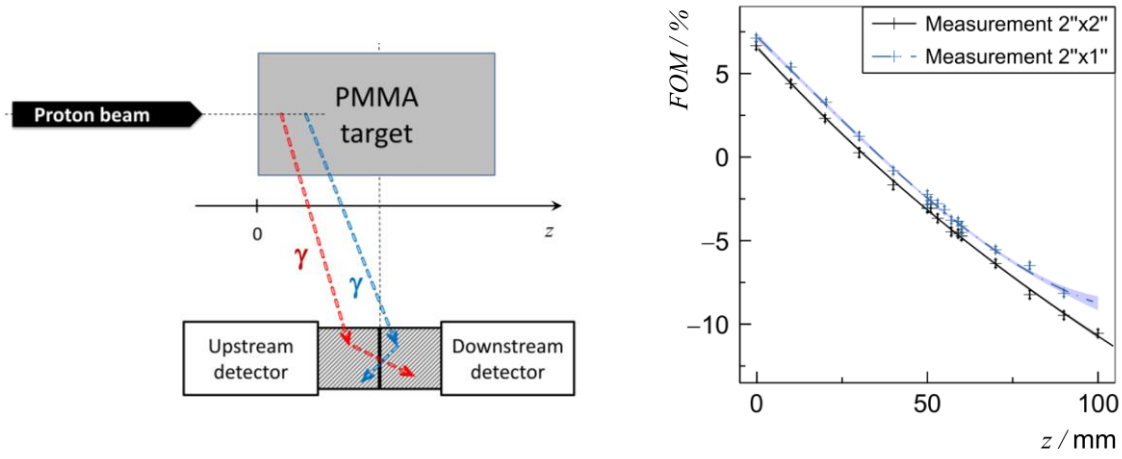

Figure 7. Sketch of the setup for testing the DGRD principle with prompt gamma rays (left panel), and Figure of Merit (right panel) denoting the relative difference of mean energies, computed for conditional spectra of the ‘upstream’ and ‘downstream’ detectors, as function of the PMMA target position [47]. The condition comprises a coincidence between both detectors, an energy cut around the 4.45 MeV sum energy peak, and an energy threshold for each detector suppressing events with energy depositions of 511 keV or less. FOM is given for two distinct measurements with PGT detection units comprising ∅2”×2” or ∅2”×1” $CeBr_3$ scintillation detectors at 90 MeV proton energy, respectively. In both cases it is well correlated with the target position.

Figure 1a

Click here to download high resolution image

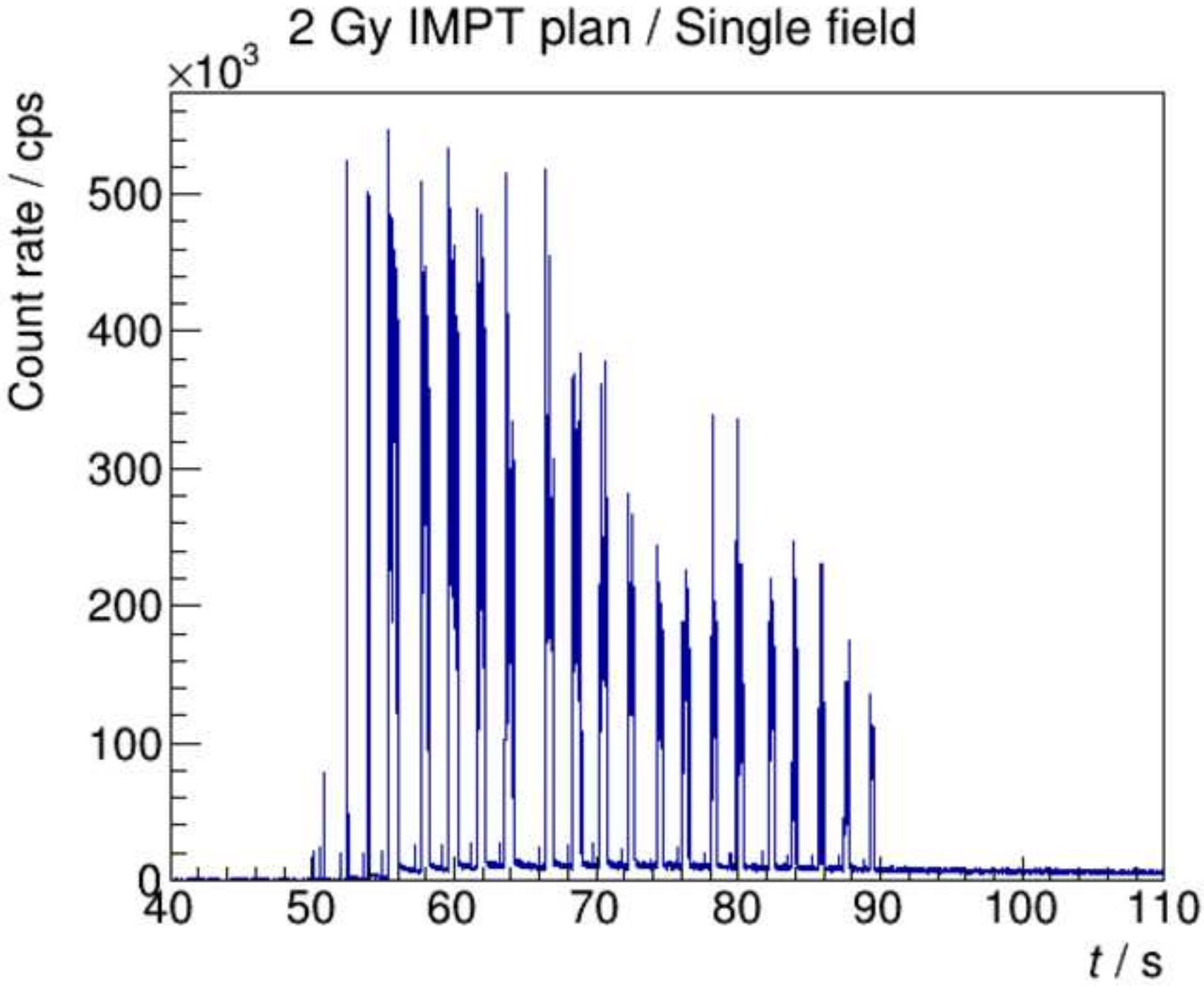

Figure 1b

Click here to download high resolution image

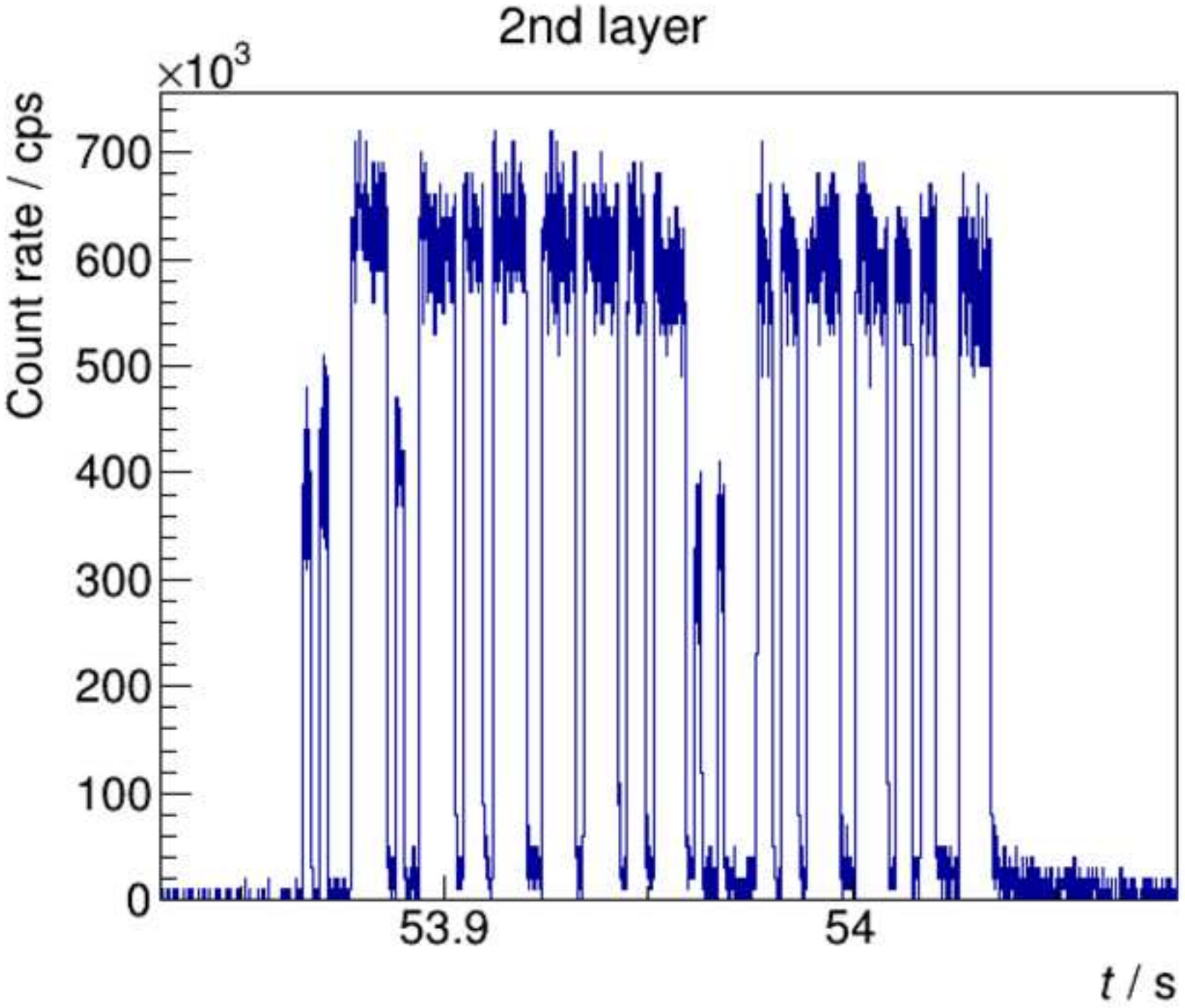

Figure 2

Click here to download high resolution image

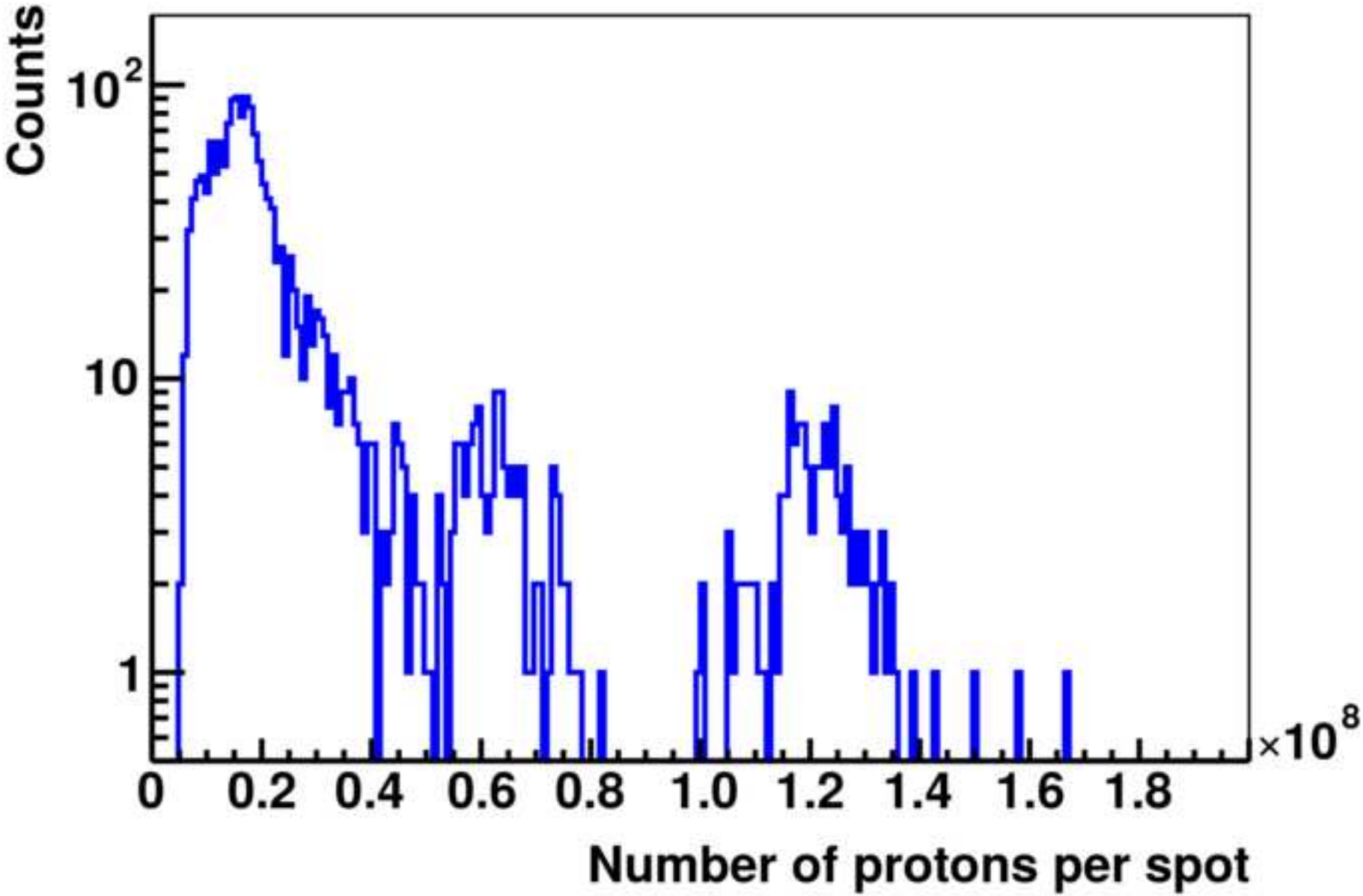

Figure 3a

Click here to download high resolution image

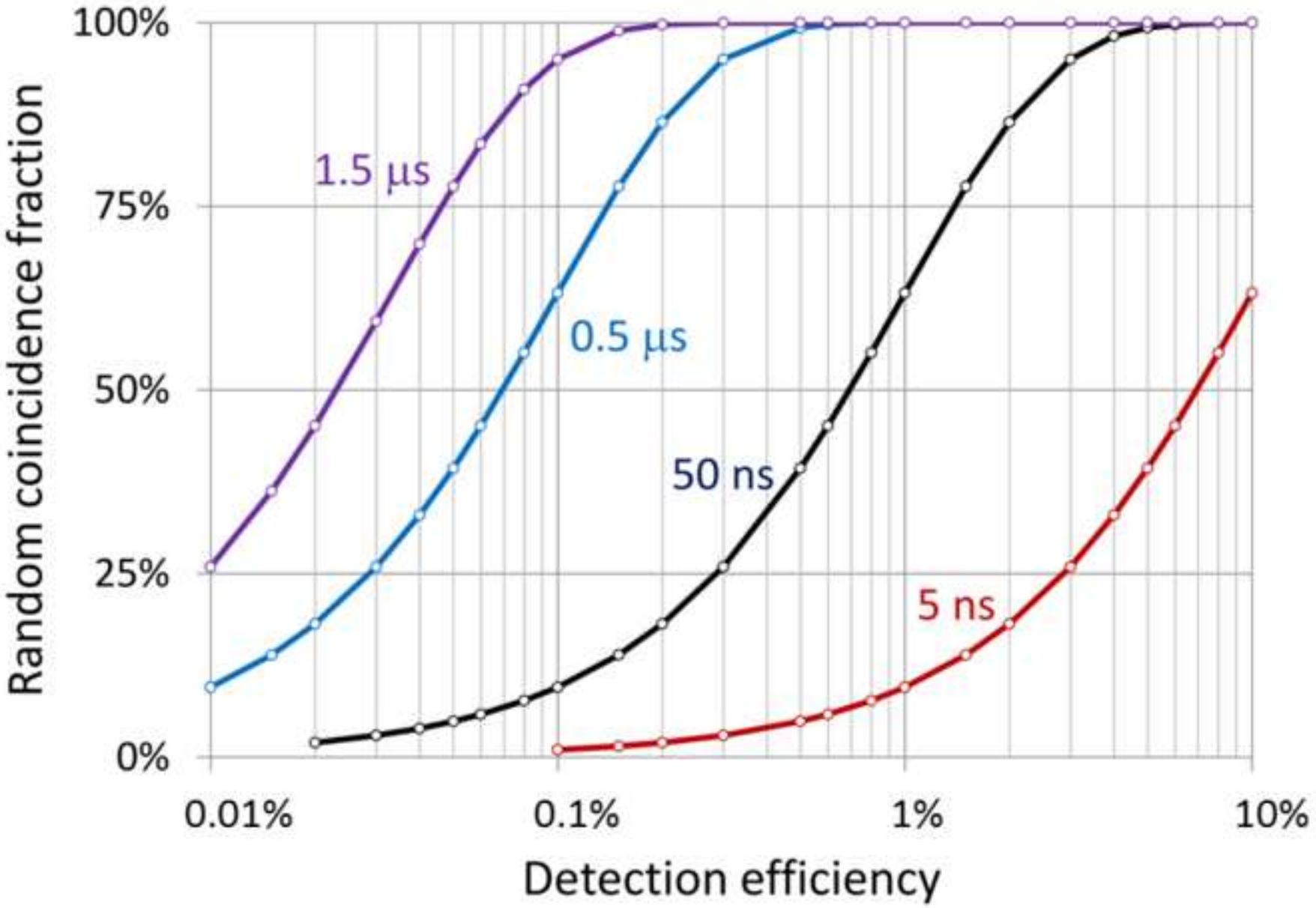

Figure 3b

Click here to download high resolution image

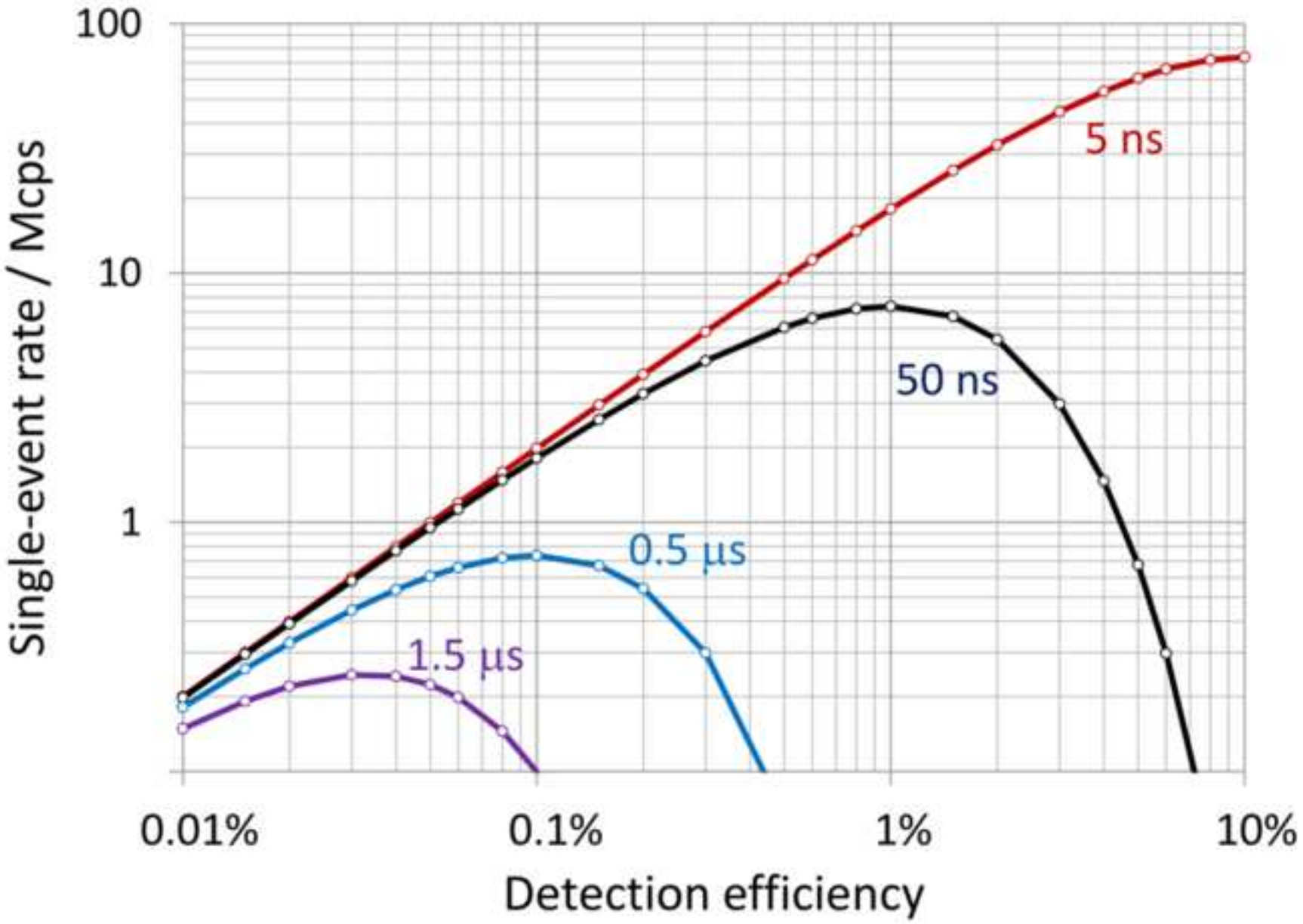

Figure 4

Click here to download high resolution image

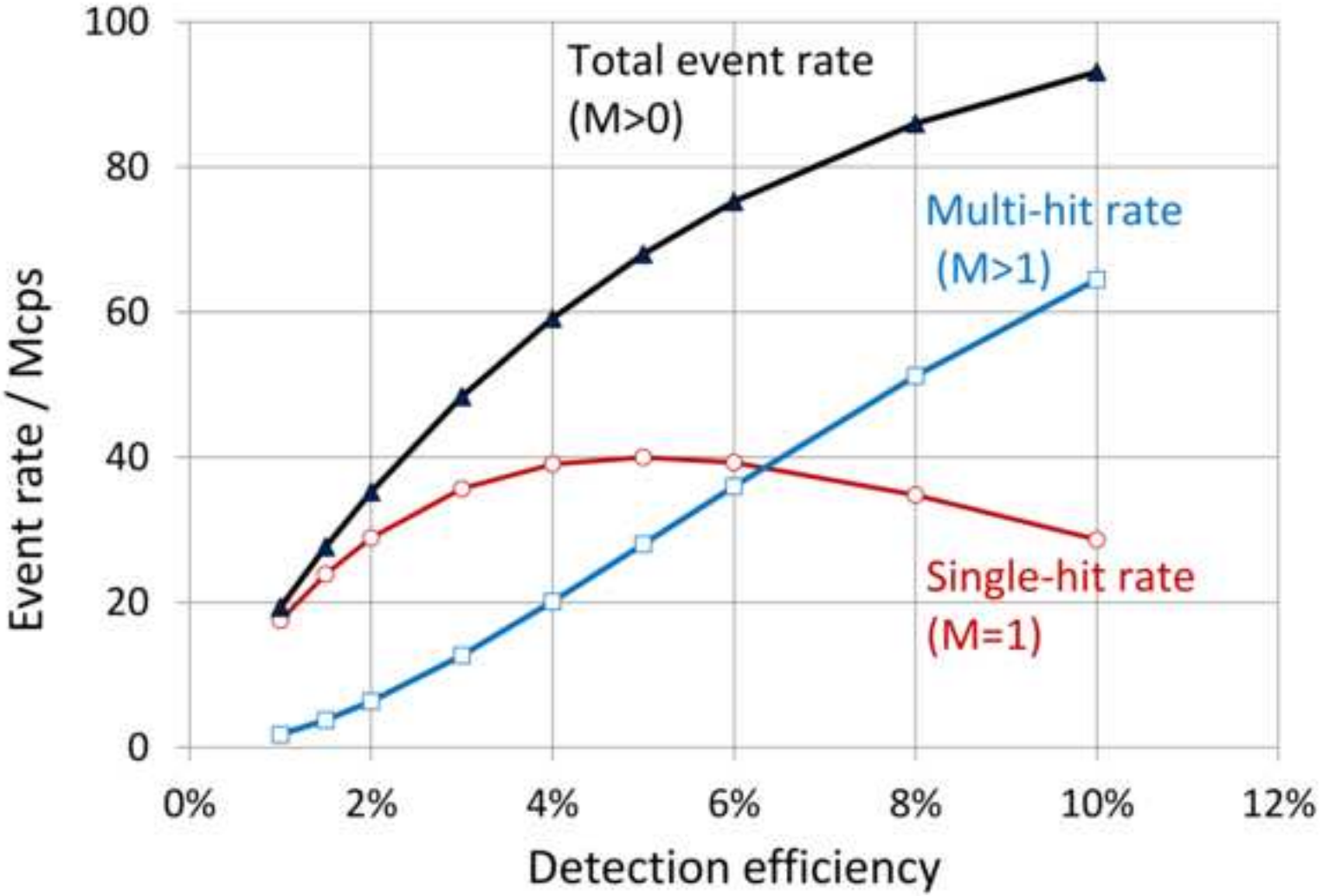

Figure 5

Click here to download high resolution image

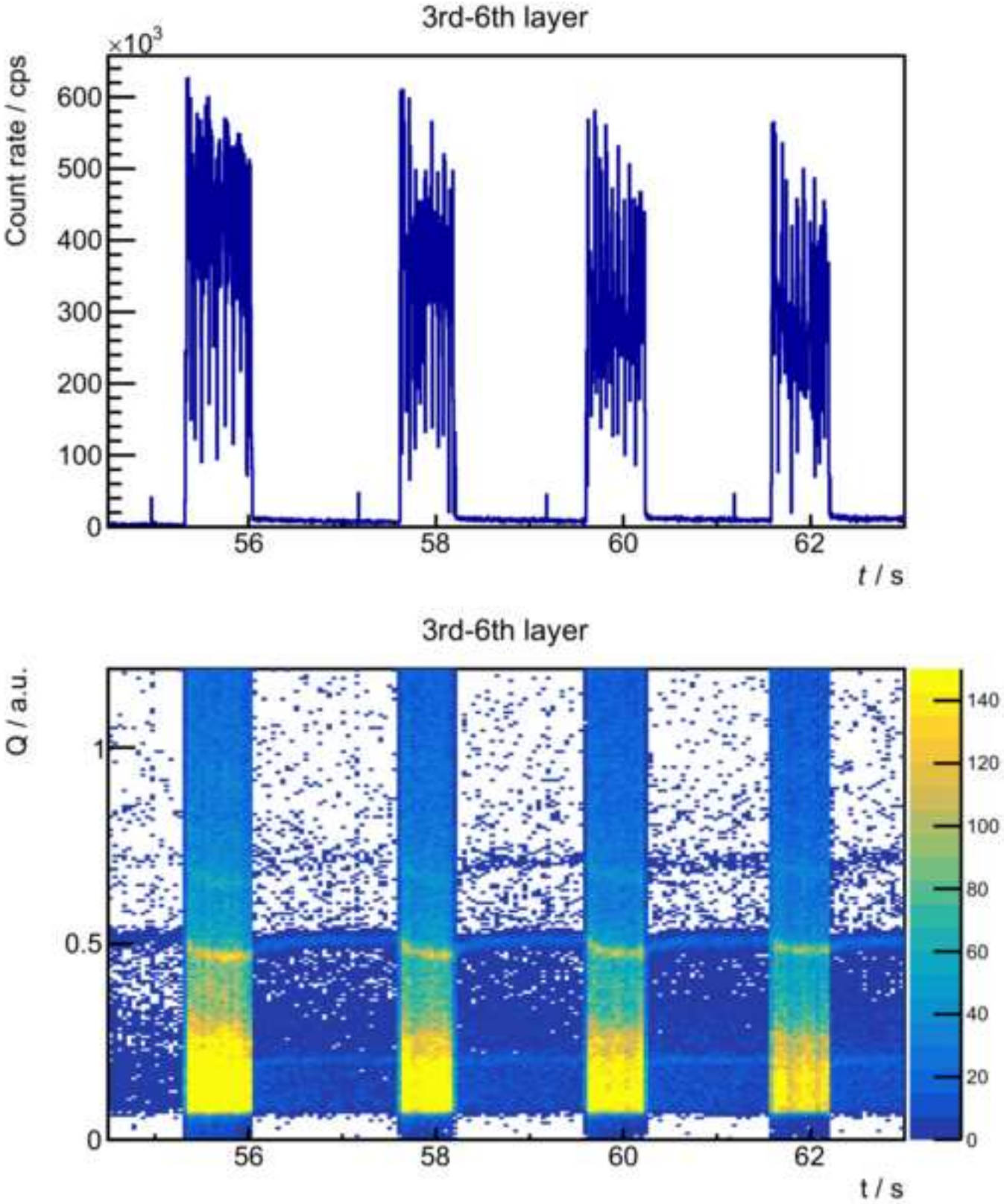

Figure 6a

Click here to download high resolution image

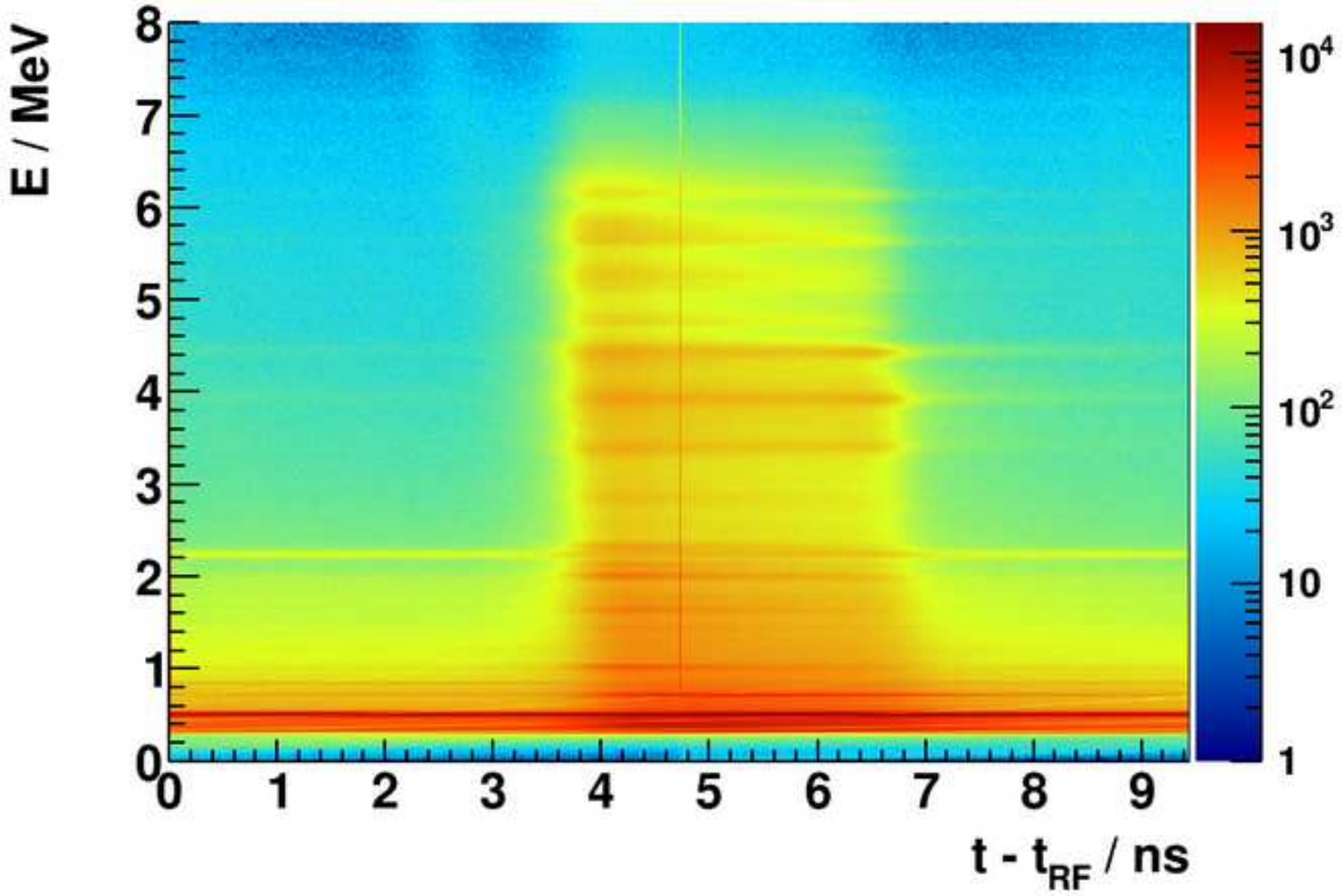

Figure 6b
Click here to download high resolution image

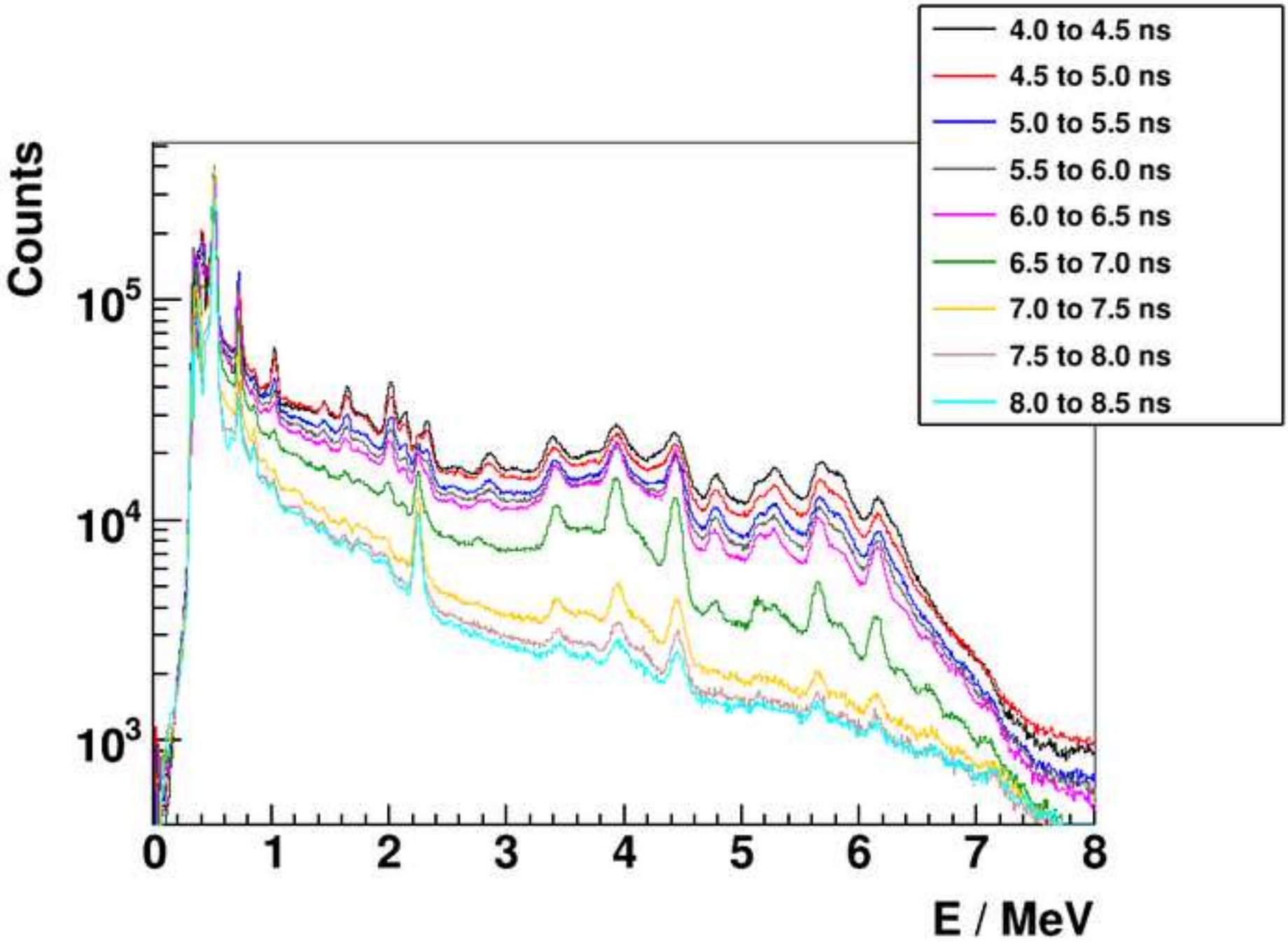

Figure 7a

Click here to download high resolution image

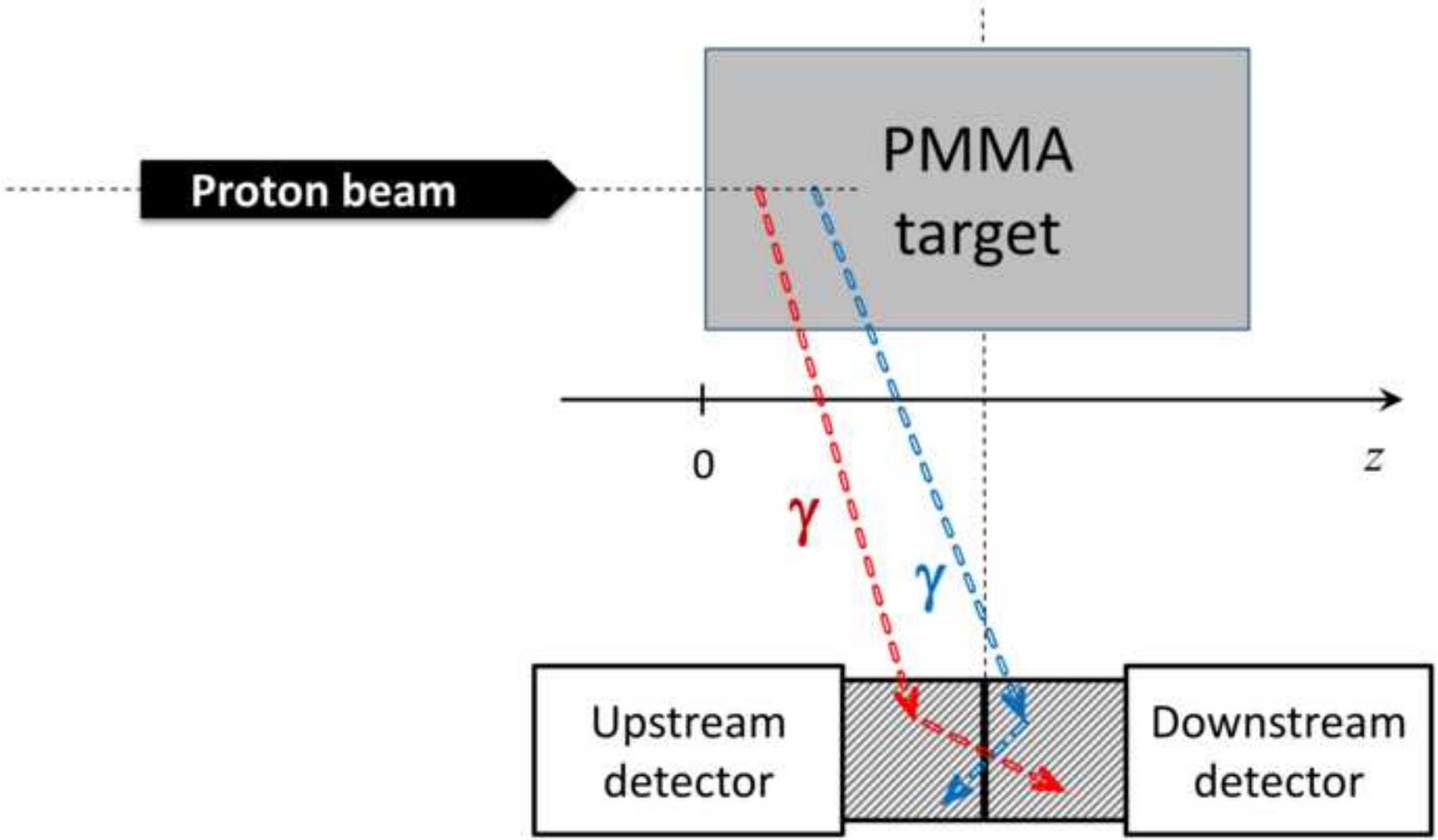

Figure 7b
Click here to download high resolution image